Review

Photocatalytic Applications of ReS$_2$-Based Heterostructures

Nan Wang, Yashu Li, Lin Wang * and Xuelian Yu *

Engineering Research Center of Ministry of Education for Geological Carbon Storage and Low Carbon Utilization of Resources, Beijing Key Laboratory of Materials Utilization of Nonmetallic Minerals and Solid Wastes, National Laboratory of Mineral Materials, School of Materials Science and Technology, China University of Geosciences (Beijing), Beijing 100083, China
* Correspondence: wanglin712@cugb.edu.cn (L.W.); xlyu@cugb.edu.cn (X.Y.)

Abstract: ReS$_2$-based heterostructures, which involve the coupling of a narrow band-gap semiconductor ReS$_2$ with other wide band-gap semiconductors, have shown promising performance in energy conversion and environmental pollution protection in recent years. This review focuses on the preparation methods, encompassing hydrothermal, chemical vapor deposition, and exfoliation techniques, as well as achievements in correlated applications of ReS$_2$-based heterostructures, including type-I, type-II heterostructures, and Z-scheme heterostructures for hydrogen evolution, reduction of CO$_2$, and degradation of pollutants. We believe that this review provides an overview of the most recent advances to guide further research and development of ReS$_2$-based heterostructures for photocatalysis.

Keywords: ReS$_2$; transition metal dichalcogenides; heterostructure; photocatalysis; photocatalytic hydrogen evolution; photocatalytic CO$_2$ reduction; photocatalytic pollutant degradation

1. Introduction

Currently, the need for clean and renewable energy sources in order to mitigate the increasing environmental pollution and global energy crisis has become more urgent. Photocatalytic technology has emerged as a promising avenue for utilizing solar energy due to its low cost, abundance, and eco-friendly nature [1]. In 1972, Fujishima and Honda demonstrated for the first time the ability to produce hydrogen by splitting water on a TiO$_2$ electrode [2]. Since then, TiO$_2$ has been extensively studied due to its strong redox abilities, eco-friendliness, and chemical stability, which have made it a promising material for photocatalysis over the past few decades [3–6]. Despite its advantages, TiO$_2$ suffers from a narrow spectral response range, a high carrier recombination rate, and a lack of catalytic active sites, thus limiting its photocatalytic hydrogen evolution (PHE) activity [7–9]. The emergence of two-dimensional (2D) photocatalysts, such as transition metal dichalcogenides (TMDs), has reinvigorated the progress in photocatalytic and photoelectrocatalytic research [10–12]. Due to their easy exfoliation into monolayers, TMDs provide numerous benefits such as a high surface area and decreased migration distance for photogenerated electron–hole pairs. This not only offers an increased number of reaction sites but also reduces the likelihood of electron–hole recombination, potentially improving photocatalytic performance [13]. Nevertheless, the electronic structure of TMDs is highly dependent on the number of layers [14]. Achieving precise control of the number of layers is critical to obtaining optimal catalytic performance, as exemplified by the fact that the photocatalytic hydrogen production of MoS$_2$ is substantially improved when it converts from a multi-layer to a single-layer configuration [15]. As such, controlling the number of layers remains a daunting task that limits the utility of TMDs in photocatalytic applications [16,17].

As a newly emerged member of the 2D TMDs family, ReS$_2$ has been widely studied in the fields of electronics [18,19], optoelectronics [20–24], and catalysis [25–28] due to its advantageous features such as a large surface area, tunable active sites, layer-independent

electric/optical properties, and structural/vibrational anisotropy. ReS$_2$ crystallizes in a twisted T phase with clusters of Re$_4$ units, forming one-dimensional chains in each single layer [29]. Distinct from the conventional 2H phase TMDs materials (represented by MoS$_2$ in Figure 1a) with high hexagonal symmetry, ReS$_2$ belongs (Figure 1b) to the triclinic crystal system with only one symmetrical center, exhibiting a distorted 1T' phase structure. The Re atoms show an octahedral coordination. The extra valence electron on the 5d orbital of Re results in a Peierls distortion, and the adjacent four Re atoms are linked by metallic bonds to form a Re$_4$ cluster, which further distorts the original hexagon of ReS$_2$ into a parallelogram [30]. It has been demonstrated that bulk ReS$_2$ consists of electronically and dynamically decoupled layers bound by weak van der Waals forces, which gives rise to a pseudo single-layer architecture with nearly identical band structures and Raman active modes compared to that of its monolayer [29,31], consequently overcoming the difficulty of preparing large-area and single-crystal monolayers. Distinct from the indirect-to-direct band-gap transition of other group-VI TMDs, both single-layer ReS$_2$ and multilayer ReS$_2$ are shown to have a direct band gap of approximately 1.4 eV (Figure 1c), with suitable band-edge positions for photocatalytic water splitting [29,32]. Additionally, the weak interlayer coupling allows for easy preparation of nanosheets with ample surface area for co-catalysis with other materials. Lastly, ReS$_2$ is significantly more adept at light absorption and carrier mobility than group-VI TMDs, thus making it an advantageous and effective photocatalyst under visible light illumination [32].
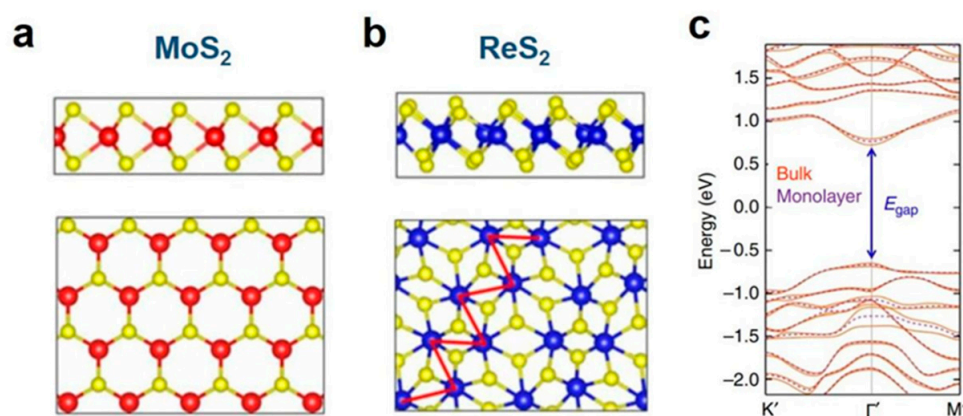

Figure 1. Top view and side view of (**a**) MoS$_2$ and (**b**) ReS$_2$. (**c**) The electronic band structure of bulk (orange solid curves) and monolayer (purple dashed curves) ReS$_2$, as calculated by DFT, is predicted to be a direct bandgap semiconductor with a nearly identical bandgap value at the Γ point [29]. Reproduced with permission: Copyright 2014, Nature Publishing Group.

In 2018, Fu's group undertook an experimental study on the optoelectronic properties of ReS$_2$ and its performance in photocatalyzed hydrogen evolution [33]. The conduction and valence band edges of ReS$_2$ are more closely spaced to the water redox potentials than CdS, thus rendering ReS$_2$ more efficient for PHE. Moreover, the monolayer-like structure of the catalyst facilitates the formation of trions (a bound state of two electrons and one hole). These trions can then migrate to the surface and participate in two-electron reactions at the abundant active sites. Furthermore, the relatively intact basal planes of ReS$_2$ can promote electron transport to the edge-reactive sites. Such a two-electron catalytic reaction endows ReS$_2$ with a PHE rate of 13.023 mmol g^{-1} h^{-1} under visible light irradiation [34].

ReS$_2$ is a versatile material but relatively less-explored among TMDs. It has garnered significant attention from the scientific community due to its unique properties compared to other TMDs. Rahman et al. critically analyzed the synthesis, structure growth mechanisms, properties, and contemporary applications of ReS$_2$ in different areas [32]. Zhang et al. has highlighted the weak coupling characteristics of ReS$_2$ [35], and the intrinsic anisotropic properties are summarized by Cao et al. [36]. Other recent reviews have summarized

advances in ReS$_2$ research with respect to electronics, optics, magnetism, and alkali-metal ion batteries [37–40]. Academic research regarding the photocatalytic properties of ReS$_2$ materials is currently limited.

It is well established that heterostructures have numerous advantages in enhancing photocatalyst functions [1,41,42]. Rational alignment of ReS$_2$ with other semiconductors into a tandem structure can increase the range of light absorption across the solar spectrum and optimize its photocatalytic performance by inhibiting charge carrier recombination as well as promoting charge separation [34,43–46]. In this review, we provide mainly an overview of the recent progress on ReS$_2$ heterostructure, focusing on the synthesis methods and their photocatalytic applications. Firstly, the preparation methods are discussed, including hydrothermal reaction, chemical vapor deposition (CVD), and mechanical or chemical exfoliation. Furthermore, we focus mainly on photocatalytic applications based on ReS$_2$-based heterostructure, such as photocatalytic hydrogen evolution, photocatalytic reduction of CO$_2$, and pollutant degradation. Finally, the review is summarized, and the prospects are discussed from current views.

2. Synthetic Methods for ReS$_2$ and Its Composite Material

Various synthesis techniques such as mechanical/chemical exfoliation, hydrothermal, and CVD methods have been developed to prepare ReS$_2$-based photocatalysts with different morphologies including nanospheres, nanosheets, etc. [45,47], all of which can be used as core components in the construction of photocatalytic heterostructures.

2.1. Exfoliation from the Bulk ReS$_2$

The weak interlayer coupling of ReS$_2$ permits the separation of bulk ReS$_2$ into nanosheets through exfoliation, which is a simple, high-yield method for ReS$_2$ preparation [29,48,49]. Ultrathin nanostructures can be obtained by employing a hybrid of mechanical and liquid exfoliation. Bulk ReS$_2$ produced using either commercial or hydrothermal synthesis can be dispersed in organic solvents (such as ethanol or N,N-dimethylformamide) through ultrasound-assisted liquid-phase exfoliation at 20–25 °C using an ice bath, followed by centrifugation and filtration to yield the nanosheets [34,47,50–53]. The bulk ReS$_2$ can be exfoliated into a few layers (Figure 2a), and the original structure of ReS$_2$ is maintained. Figure 2b,c show the intact basal plane and edge of ReS$_2$ nanosheets, respectively [50]. Figure 2d,e display the ReS$_2$ nanosheets with a thickness of about 4.20 nm [54]. The under-coordinated sulfur sites at the edges of ReS$_2$ nanosheets serve as highly active centers for H$_2$ generation, while the intact basal plane facilitates efficient electron transport to these edge S active sites for H$_2$ evolution [34]. Chemical methods, such as the addition of diazonium salts, can also be employed to modify the surface structure of TMDs during the stripping process [55]. For example, the incorporation of hydroxyl functional groups such as carboxyl can enhance the hydrophilicity of ReS$_2$ and improve its dispersibility in the ReS$_2$−C$_6$H$_5$COOH/TiO$_2$ physical mixture, thus preserving the photocatalytic active sites [56].
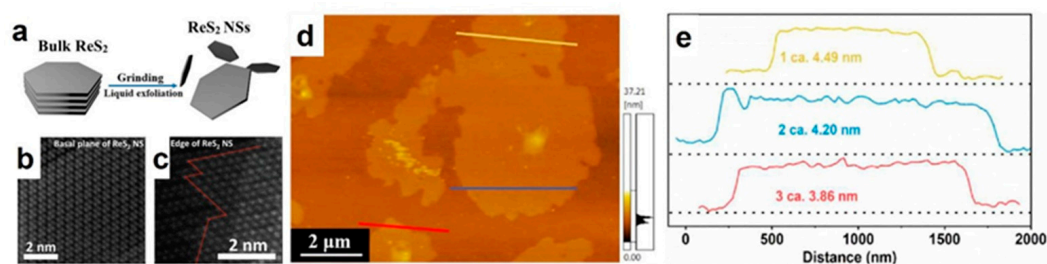

Figure 2. *Cont.*

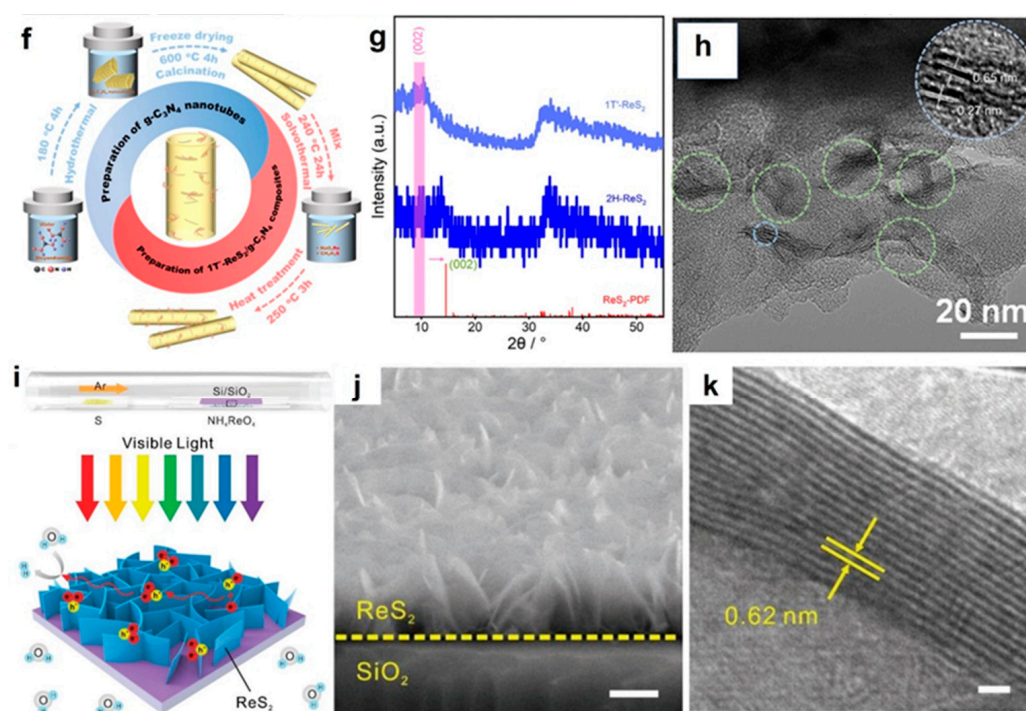**Figure 2.** (**a**) Liquid exfoliation of ReS$_2$ nanosheets from bulk material [47]. Reproduced with permission: Copyright 2019, IOP Publishing. Atomic-resolution HAADF-STEM images of (**b**) basal plane and (**c**) edge of ReS$_2$ nanosheets [50]. (**d**) AFM image and (**e**) thickness profiles of ReS$_2$ nanosheets [54]. Reproduced with permission: Copyright 2021, Wiley-VCH Verlag GmbH & Co. KGaA. (**f**) Schematic illustration of the solvothermal synthesis process of g-C$_3$N$_4$ nanotubes and 1T'-ReS$_2$/g-C$_3$N$_4$ composites [57]. Reproduced with permission: Copyright 2022, ELSEVIER. (**g**) XRD patterns of 1T'-ReS$_2$ and 2H-ReS$_2$ after heat treatment [57]. (**h**) TEM images of 1T'-ReS$_2$/g-C$_3$N$_4$ composite (12 wt%) [57]. Reproduced with permission: Copyright 2022, ELSEVIER. (**i**) Schematic diagram of the CVD-synthesized ReS$_2$ and the two-electron photocatalytic reaction [33]. (**j**) SEM image of the lateral view of the ReS$_2$ nanowalls on the silicon substrate; scale bar: 200 nm [33]. (**k**) HRTEM characterization of a ReS$_2$ NW with clear lattice fringe; scale bar: 2 nm [33]. Reproduced with permission: Copyright 2018, Wiley-VCH Verlag GmbH & Co. KGaA.

2.2. Hydrothermal Synthesis Reaction

The hydrothermal method is one of the simplest methods for the preparation of TMDs [16]. Specific precursors are used to carry out chemical reactions under high temperature and high pressure in a specially designed polytetrafluoroethylene-lined autoclave. For the synthesis of pristine ReS$_2$, ammonium perrhenate (NH$_4$ReO$_4$), hydroxylamine hydrochloride (NH$_2$OH·HCl), and thiourea (CS(NH$_2$)$_2$) are dissolved in deionized water. After stirring, they are transferred to a polytetrafluoroethylene autoclave for hydrothermal reaction by heating to 200–240 °C for 12–48 h [58–60]. After cooling, the ReS$_2$ black powder is repeatedly washed with deionized water and ethanol, and the final product is collected after drying. The ReS$_2$ prepared using this method typically displays the morphology of nanospheres, and the size of the ReS$_2$ nanospheres can be adjusted by regulating the concentration of rhenium sources in the reaction [45].

The enhanced photocatalytic activity of ReS$_2$ can be achieved by combining it with another semiconductor material to construct heterojunctions [61]. There are two ways to prepare ReS$_2$-based heterojunctions via the hydrothermal method. The first is to incorporate the synthesized host semiconductor material into the precursor mixture for the preparation of ReS$_2$, or vice versa, using a two-step hydrothermal method [46,62]. Wang et al. dispersed the generated TiO$_2$ nanofibers into the ReS$_2$ preparation solution for the hydrothermal reaction to anchor the ReS$_2$ nanosheets on the porous TiO$_2$ nanofibers to form TiO$_2$@ReS$_2$ composites. The few-layer ReS$_2$ nanosheets with twisted 1T phase that were prepared

via the hydrothermal method show large catalytic active sites, high electron mobility, and matching band structure [58]. The other is to fabricate a heterostructure with all the raw material in the one-pot hydrothermal method [63]. Chen et al. prepared a 1T'-ReS$_2$/g-C$_3$N$_4$ heterostructure via the one-pot solvothermal reaction (Figure 2f). The obtained 1T'-ReS$_2$ nanosheets can be converted to 2H-ReS$_2$ after subsequent heat treatment (Figure 2g). The thin 1T'-ReS$_2$ nanosheets with multi-layers grown on the g-C$_3$N$_4$ nanotubes (green circle in Figure 2h) show characteristic 2D-layered structures of TMDs with the single-layer thickness ~0.27 nm and the interlayer spacing ~0.65 nm (blue circle in Figure 2h). Alternatively, ReS$_2$ prepared via the hydrothermal method can also be subsequently combined with other semiconductor materials through grinding or liquid-phase dispersion, thereby enabling the construction of heterojunctions [51,64].

2.3. Chemical Vapor Deposition Technique

ReS$_2$ nanosheets prepared through hydrothermal and exfoliation methods contain numerous impurities that can act as electron-and-hole recombination centers, thus reducing the photocatalytic activity of ReS$_2$ [65]. Compared to other methods, CVD-prepared TMDs have many advantages, including uniform appearance, controllable thickness, low defect rate, clean interface, and high synthesis efficiency [66,67]. On the one hand, the weak van der Waals interaction between TMDs makes it possible to stack them to form a variety of vertical heterostructures. On the other hand, chemical bonds can be formed at the interface to realize the interlocking of different 2D materials to form horizontal heterostructures with special interfacial properties. Vertical heterostructures can be prepared through methods such as mechanical exfoliation and transfer [68,69], direct CVD growth [70], electrochemical exfoliation [71], and liquid-phase exfoliation [47]. Horizontal heterostructures can generally be prepared only by the CVD approach [72–74].

The CVD preparation of ReS$_2$ heterostructures can also be divided into a "one-step method" and a "two-step method". The one-step method puts the precursor containing the elements of the synthesized heterostructure into the reaction system at one time. This method is based on the difference in the substrate adsorption energy or the control of growth conditions, such as growth temperature or carriers, to realize the growth of two materials one after another. For example, by utilizing the difference in adsorption energy between Re and W atoms on a Au substrate, a one-step synthesis of a vertical ReS$_2$/WS$_2$ heterojunction on a Au/W-Re alloy foil can be achieved [75]. The two-step method means that the growth of heterostructures is carried out in two separated steps. These methods can realize the high-quality and large-area preparation of single-crystal ReS$_2$, which has been widely used in micro-nano electronic devices and photoelectric detection fields [22,23,76]. A substantial amount of work has reported the CVD preparation and growth mechanism of ReS$_2$ heterostructure; readers can refer to the related papers [72–75,77,78] and reviews [79].

The majority of TMDs produced via CVD techniques exhibit a parallel growth relative to the underlying substrate, resulting in a flat film morphology. Under similar CVD growth conditions, ReS$_2$ nanosheets display a propensity to bend and adopt a vertically oriented configuration on the underlying substrate [80]. Specifically, the vertical growth of two-dimensional ReS$_2$ is highly spontaneous and independent of the substrate [81]. The high packing density ($\sim 10^8$ cm^{-2}) of the ReS$_2$ nanosheets promotes a substantial number of active Re atoms to be exposed at the sheet edges, providing abundant active sites for catalytic processes [33,70,80,82–84]. The common precursors for the CVD synthesis of ReS$_2$ are ammonium rhenate (NH$_4$ReO$_4$), Re powder [82], and rhenium-containing oxides (ReO$_3$ or Re$_2$O$_7$), with sulfur powder used as the predominant sulfur source and heated in a different zone [33,85,86]. The ReS$_2$ prepared via the CVD method exists mostly in petal-like ReS$_2$ nanowalls arranged vertically without agglomeration [28,33,87]. Zhang et al. anchored the ReS$_2$ nanowalls vertically on the surface of the Si/SiO$_2$ substrate (Figure 2i), which can distribute ultra-uniformly with a dense structure over a wide area (Figure 2j) [33]. The average length of the ReS$_2$ nanowalls can be up to 200 nm with domain sizes of about 10 layers. The interplanar distance of the ReS$_2$ nanowalls is about 0.62 nm

(Figure 2k), corresponding to the (001) crystal plane. The beneficial exposure of the (001) facet ensured that more active sites were accessible for hydrogen adsorption, consequently enhancing the catalytic activity. The growth of the ReS_2 single-crystal nanosheets does not need a polished substrate or a small lattice mismatch [87]. Cheng et al. grew ReS_2 tightly on the TiO_2-coated b-Si substrate with the shape of nanopyramids via the CVD method. The obtained ReS_2 nanosheet was of high quality and exhibited a good crystal structure without defects [28]. Before the characterization of photocatalytic properties, ReS_2 generally needs to be scraped off from the substrate, and then via the solution reaction (such as hydrothermal or self-assembly) to prepare heterostructures.

3. Heterostructured ReS_2 Composites

The heterojunctions formed between the host semiconductors generate an internal electric field that facilitates the separation of electron–hole pairs and accelerates the migration of carriers, which is constructive for improving the photocatalytic efficiency [88–90]. ReS_2-based heterostructures can fulfill the aforementioned requirements and demonstrate outstanding photocatalytic performance. According to the bandgaps and the electronic affinity of semiconductors, ReS_2-based heterostructures can be divided into three different types: type-I (straddling gap), type-II (staggered gap), and Z-scheme system, the band alignment of which is shown in Figure 3. The band gap, the electron affinity, and the work function of the combined semiconductors can determine the dynamics of the electron and hole in the semiconductor heterojunctions.
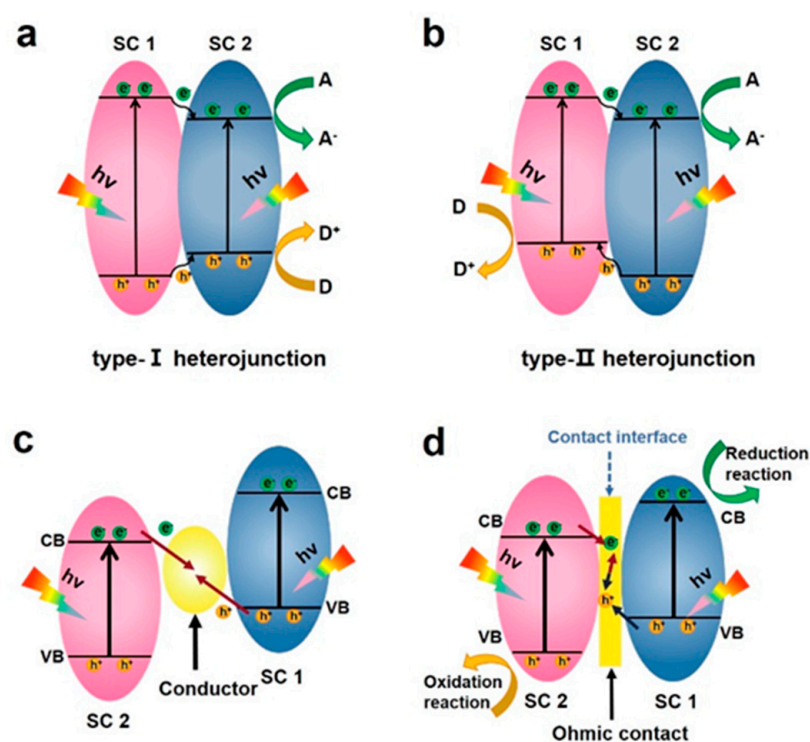

Figure 3. Diagram of (**a**) Type-I, (**b**) Type-II, and (**c**) all-solid-state Z-Scheme heterojunction. (**d**) Direct Z-scheme heterojunction.

3.1. Type I Heterostructure

In a type-I heterostructure (shown in Figure 3a), the photo-excited electrons and holes in the wide-gap material transfer to the narrow-gap material (ReS_2), as demonstrated by the arrows [46,50,51,53,54,91–93]. The quantum confinement of the accumulated electrons and holes in the same semiconductor facilitates high carrier recombination rate and radiative recombination, which is incredibly detrimental to photocatalytic activity but desirable in light-emitting applications [91,94]. To inhibit recombination of photo-generated charge,

a cocatalyst such as Pt that is deposited in situ onto the surface [54] or abundant sulfur vacancies [93] can act as an electron trapper to facilitate electron accumulation and transfer. Additionally, the abundant edge reaction sites in ultrathin ReS_2 nanosheets in the composites can also accumulate electrons, thus accelerating reaction kinetics of the hydrogen evolution [53].

3.2. Type II Heterostructure

In a type-II heterojunction semiconductor, both valence band (VB) and conduction band (CB) of semiconductor 1 are situated at higher energy levels than those of semiconductor 2 (Figure 3b). The alignment of the energy levels facilitates electrons transferring from semiconductor 1 to semiconductor 2, while the holes migrate in the opposite direction. If both semiconductors are in close contact, an effective charge separation will take place upon light illumination. This leads to a decrease in charge recombination and an increase in the lifetime of charge carriers, resulting in higher photocatalyst activity. As one of the typical systems, the VB and CB of MX_2 are both higher than that of ReS_2. They can form a Type-II heterojunction structure in which the electrons transfer to ReS_2 with holes transferred to MX_2 [21,95,96]. Zhang et al. constructed a type-II heterojunction between ReS_2 and XS_2 (X = Mo, W), which can promote the electron transfer to further improve the photocatalytic performance of the counter electrode in dye-sensitized solar cells [96].

Traditional type-II heterojunctions (including n–n junctions and p–n junctions) have several obvious limitations. (1) From the thermodynamic point of view, the improvement of charge separation efficiency is at the expense of oxidation/reduction ability. Specifically, photo-generated electrons will accumulate on the CB of semiconductor 2 with a weaker reduction potential, and photo-generated holes will accumulate on the VB of semiconductor 1 with a lower oxidation potential. Following the type-II charge transfer mechanism, it will inevitably weaken the thermodynamic driving force of the photocatalytic reaction. (2) In terms of dynamics, the transition electrons of semiconductor 2 and the electrons transferred from semiconductor 1 will produce repulsive force. Similarly, the holes between them will also repel each other, which greatly hinders the continuous charge transfer in the type-II heterostructure. (3) Finally, the electrostatic attraction of electrons in semiconductor 2 and holes in semiconductor 1 also render the interfacial charge transfer of type-II composites difficult to achieve [61].

3.3. Z-Scheme Heterojunction

Thanks to inspiration from natural photosynthesis, in which two-step photoexcitation and electron transfer are connected in series to form a letter "Z", similar artificial bionic Z-type heterostructures have been studied and developed in the photocatalysis field [97,98]. The first generation of the liquid-phase Z-scheme system has shuttle oxidation/reduction medium pairs, which are played by electron acceptor/donors, respectively, while there is no physical contact between oxidized semiconductors and reduced semiconductors. However, the first-generation Z-scheme photocatalytic system is limited to use in liquid-phase reactions, severely constraining its practical applications in gas- or solid-phase processes [99]. The second-generation all-solid-state Z-scheme heterojunction uses solid conductors (generally noble metal nanoparticles) instead of redox pairs to make it suitable for both liquid–solid and gas–solid reactions (Figure 3c). After the two semiconductors are excited at the same time, the electrons on the CB of the oxidized semiconductor will migrate to the solid conductor and then transfer to the VB of the reduced semiconductor. The length of this charge transfer path is significantly shortened compared to the initial liquid-phase Z-type heterostructure, which can greatly accelerate the charge transfer and separation efficiency. However, due to the difficulty in accurately controlling the heterojunction structure, the difficulty in directional electron transfer on the interface, and the competition between the light absorption of the mediator itself and the main catalytic components, these two heterostructures have not achieved the ideal photocatalytic effect [100].

The third-generation direct Z-type heterojunction is composed of only a reduced semiconductor and an oxidized semiconductor with a matching band structure and an ohmic contact at the interface (Figure 3d). This ohmic contact interface has certain defects and can be used as a recombination center for the electrons on the CB of the oxidized semiconductor and the holes on the VB of the reduced semiconductor. In addition, the impurity orbits contribute quasi-continuous energy levels and become charge transfer mediators. In addition to inheriting the advantages of the first two generations of Z-scheme systems, the direct Z-scheme without a solid medium greatly reduces the construction cost. Meanwhile, the direct Z-type heterostructure overcomes the light-shielding effect caused by redox pairs or noble metal particles [101]. Although the resistance of the direct Z-scheme at the solid–solid interface is generally considered to be higher than that of the all-solid-state Z-scheme, it is often possible to improve the conductivity of the interface by regulating or optimizing the chemical-binding force through molecular polarization to maximize the advantages of the Z-scheme heterojunction [56].

4. Photocatalytic Applications of Heterostructure ReS_2

The direct band gap of ReS_2 in both monolayer and bulk form is approximately 1.4 eV [29], allowing for the absorption of light across the entire visible spectrum and into the near-infrared region, making it an ideal material for visible light photocatalysis. The weak interlayer coupling of ReS_2 results in optoelectronic properties that are largely independent of the number of layers, and the unsaturated edge sites are particularly exposed [35]. These advantages endow ReS_2 with considerable potential as an efficient photocatalyst or cocatalyst. Considering the limitations of a single photocatalyst, coupling other semiconductors with ReS_2 into heterojunctions can not only improve the utilization of solar energy but also reduce electron–hole pair recombination, thereby improving redox capacity. ReS_2-based heterostructure composites have provoked extensive research attention and exhibit excellent photocatalytic activity in the fields of hydrogen production, CO_2 reduction, and pollutant degradation.

4.1. Photocatalytic Hydrogen Production

Hydrogen, which is generated from photocatalytic water splitting, has been regarded as a potential source of energy for the development of a sustainable economy and society. Qualified photocatalysts should have a bandgap over 1.23 eV. The conduction band minimum (CBM) should be higher in energy than the H^+/H_2 water reduction potential, while the valence band maximum (VBM) should be lower in energy than the OH^-/O_2 water oxidation potential. The band-gap and band-edge positions of monolayer and multilayer ReS_2 are highly compatible with the energy levels required for water splitting [102]. Pioneer work by Zhang et al. reported that a multilayer structure ReS_2 with monolayer-like features can generate a tremendous number of trions consisting of two electrons and one hole. This can trigger a two-electron catalytic reaction, offering a PHE rate of 13 mmol g^{-1} h^{-1} under visible light, which is larger than that of most reported TMD composite photocatalysts [33]. Due to its distorted 1T phase structure, transition metal σ bond, and direct band gap, ReS_2 can serve as an electron reservoir with fast electron transport speed and active electronic states. Consequently, ReS_2 has been widely recognized as an excellent cocatalyst for constructing a heterostructure with classical photocatalysts such as TiO_2 [27,34,58,103,104], CdS [44,45,59,62], and g-C_3N_4 [46,54,57,92]. It can not only markedly enhance the visible light absorption, charge transfer, and carrier separation efficiency but also offer abundant edge active sites. Additionally, when Re vacancy is produced in ReS_2, some unsaturated S atoms around the defect sites can promote the adsorption of a H^+ proton, thus improving the HER performance more than perfect ReS_2 [34,53,60]. The performance for ReS_2 as a cocatalyst has been reported to be comparable to widely used noble-metal cocatalysts such as Pt [44,57]. Various photocatalysts have been summarized in Table 1 on the water splitting for the H_2 production.

Table 1. Applications of ReS_2-based heterostructure for hydrogen production.

Photocatalyst	Source of Light	Morphology	Performance	Ref
$ReS_2/ZnIn_2S_4$	300 W Xenon arc lamp ($\lambda \geq 420$ nm cutoff filter)	cobblestone structure with particles	1858.6 μmol h^{-1} g^{-1}	[61]
ReS_2 nanowalls	300 W Xenon arc lamp ($\lambda \geq 420$ nm cutoff filter)	ReS_2 nanowalls	13 mmol h^{-1} g^{-1}	[33]
TiO_2/ReS_2	300 W Xenon arc lamp	ReS_2 nanosheets and TiO_2 nanofibers	1404 μmol h^{-1} g^{-1}	[58]
ReS_2/TiO_2	Solar simulator ($\lambda \geq 300$ nm)	sea-urchin-like structured	3.71 mmol h^{-1} g^{-1}	[104]
ReS_2-BzO-TiO_2	Solar simulator	nanosheets	9.5 mmol h^{-1} g^{-1}	[56]
CdS/ReS_2	300 W Xennon lamp ($\lambda \geq 420$ nm UV-cutoff filter)	nanorod	137.5 mmol h^{-1} g^{-1}	[59]
$ReS_2/Zn_{0.5}Cd_{0.5}S$	visible light irradiation ($\lambda \geq 420$ nm)	nanospheres on ReS_2 nanosheets	112.10 mmol h^{-1} g^{-1}	[105]
$ReS_2/Mn_{0.2}Cd_{0.8}S$	300 W Xenon arc lamp ($\lambda \geq 420$ nm cutoff filter)	cauliflower-like morphology	17.31 mmol h^{-1} g^{-1}	[43]
$CdS/(Au-ReS_2)$	300 W Xenon arc lamp ($\lambda \geq 420$ nm cutoff filter)	ReS_2 nanosheets	3060 μmol h^{-1} g^{-1}	[45]
g-$C_3N_4/CdS/ReS_2$	300 W Xenon arc lamp (AM 1.5 G filter)	a hollow spherical nano-shell structure	7141.2 $\pm$ 85.7 μmol h^{-1} g^{-1}	[44]
$ReS_2/ZnIn_2S_4$-S_v	300 W Xenon arc lamp	nanoflower	1.08 mmol h^{-1} g^{-1}	[93]
ReS_2/TiO_2	300 W Xenon arc lamp	ReS_2 ultrathin nanosheets	1037 μmol h^{-1} g^{-1}	[34]
ReS_2/g-C_3N_4	Solar simulator (AM 1.5G)	nanospheres	1823 mmol h^{-1} g^{-1}	[92]
$ReS_2/ZnIn_2S_4$	Xenon arc lamp (400 nm cutoff light filter)	ReS_2 nanosheets	2515 μmol h^{-1} g^{-1}	[50]
ReS_2/g-C_3N_4	300 W Xenon arc lamp	ultrathin layered 2D/2D structure	3.46 mmol h^{-1} g^{-1}	[54]
$MoS_2/ReS_2@CdS$	300 W Xenon arc lamp ($\lambda \geq 420$ nm)	$CdS@ReS_2$ nano-spheres and MoS_2 nanoflakes	171.9 mmol h^{-1} g^{-1}	[63]
ReS_2/TiO_2	300 W Xenon arc lamp	circle-shaped sheet-like structures 2D TiO_2	762.3 mmol h^{-1} g^{-1}	[103]
ReS_2/g-C_3N_4	visible light irradiation ($\lambda \geq 420$ nm)	ReS_2 nanoflowers on the surface of g-C_3N_4	249 μmol h^{-1} g^{-1}	[46]
ReS_2-CdS/P-0.2	300 W Xenon arc lamp ($\lambda \geq 420$ nm cutoff filter)	CdS nanorods and ReS_2 nanosheet	14.68 mmol h^{-1} g^{-1}	[62]
Ta_3N_5/ReS_2	300 W Xenon arc lamp	CdS nanorods and ReS_2 nanosheet	615 μmol h^{-1} g^{-1}	[53]

The morphology and structure of cocatalysts are important factors that can influence the photocatalytic performance. Cocatalysts typically exhibit morphologies such as nanoparticles, nanospheres, flakes, clusters, nanotubes, and quantum dots. Inspired by nature, Lin et al. designed novel sea-urchin-like ReS_2 nanosheet/TiO_2 nanoparticle heterojunctions through a simple one-pot hydrothermal method (Figure 4). Compared with the bulk ReS_2 cocatalyst composed of a large number of agglomerated nanoparticles or nanosheets, the sea-urchin-like ReS_2 cocatalyst shows a significantly accelerated charge transfer due to the unusual charge edge-collection effect. The photocatalytic H_2 evolution rate is 3.71 mmol h^{-1} g^{-1} (an apparent quantum efficiency (AQE) of 16.09%), which is 231.9 times that of P25 TiO_2 [104].
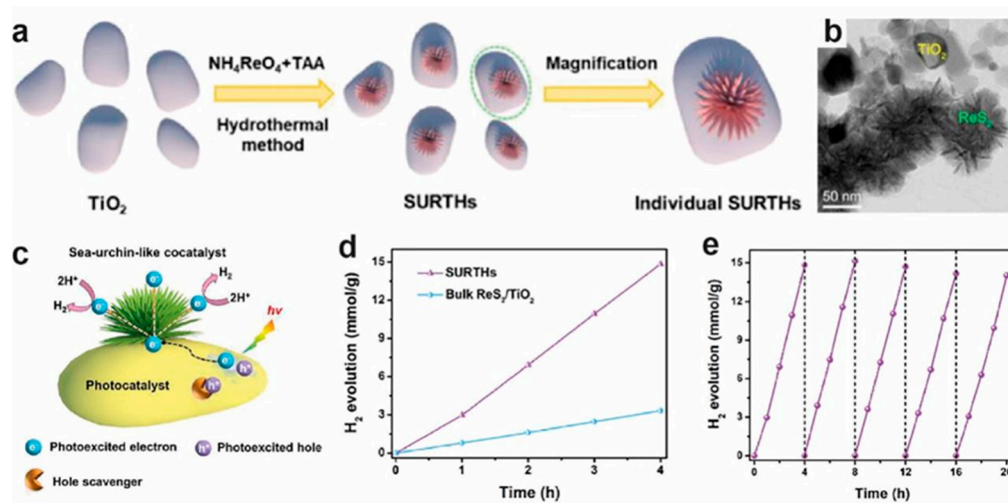
Figure 4. (**a**) The formation procedure of ReS$_2$ nanosheet/TiO$_2$ nanoparticle heterojunctions (SURTHs). (**b**) TEM images of SURTHs (**c**) Schematic of the sea-urchin-like cocatalyst with the charge edge-collection effect loaded on the photocatalyst for H$_2$ evolution. (**d**) Time-dependent photocatalytic hydrogen production of Bulk ReS$_2$/TiO$_2$ and SURTHs under simulated solar-light irradiation. (**e**) Cycling tests for photocatalytic hydrogen production over SURTHs under simulated solar-light irradiation [104]. Reproduced with permission: Copyright 2022, ELSEVIER.

TMDs with a metallic 1T phase and semi-metallic 1T' phase generally have high electrical conductivity [106,107]. However, most TMDs with the 1T-phase and 1T'-phase are thermodynamically unstable and can easily convert to the sTable 2H-phase [108,109]. Inspiringly, ReS$_2$ has a thermodynamically sTable 1T'-phase crystal structure, which shows great promise for better catalytic performance [32,58]. As cocatalysts, the conductive 1T'-ReS$_2$ nanosheets can trigger the host g-C$_3$N$_4$ nanotubes to generate more photoexcited charges, promote the carrier migration and separation, and supply abundant active sites for photocatalysis. Thus, the 1T'-ReS$_2$/g-C$_3$N$_4$ composite containing 12 wt% 1T'-ReS$_2$ exhibits an excellent photocatalytic H$_2$ evolution rate of 2275 mmol h^{-1} g^{-1} [57]. Regulating phase structure and constructing an in-plane heterostructure of ReS$_2$ can also provide more active sites and increase electron transfer [26]. Chen et al. reported that simply phosphorization treatment led to a shift in the Fermi level due to the extra electrons filling in the d orbital, and thus, ReS$_2$ partially transformed from the T' to the T phase [62]. The developed 2% ReS$_2$-CdS/P-0.2 photocatalyst with in-plane T-T' heterophase junctions enhanced the interfacial effect between CdS and ReS$_2$, which can facilitate the electron transfer and exhibit an optimal hydrogen generation rate of 14.68 mmol g^{-1} h^{-1}.

Heterostructures with well-identified interfaces are crucial for enhancing photocatalytic performance. The intimate interfacial contact between the individual components via the covalent bond can greatly accelerate the separation of photogenerated electrons and holes. Taking the TiO$_2$@ReS$_2$ nanocomposites for example, the photoexcited electrons can rapidly transfer to ReS$_2$ and diffuse to the active sites due to the chemical interaction of the Ti−O−Re bond [58]. The optimized TiO$_2$@ReS$_2$ nanocomposites with 30 wt% ReS$_2$ exhibit superior photocatalytic H$_2$ evolution activity with a rate of 1404 μmol h^{-1} g^{-1}. In another 2D/2D heterostructure, the cocatalyst ReS$_2$ with abundant active sites is strongly anchored on the TiO$_2$ by the chemical interaction of the Ti–S bond, and the established intimate interfacial contact facilitates efficient carrier transfer across the interface [103]. Recently, the strongly coupled interface between atomic-level regulated ReSe$_2$ and various semiconductor photocatalysts and the abundant Re/Se active sites have been demonstrated to boost the performance for photocatalytic H$_2$ evolution [110].

Table 2. Applications of ReS_2-based heterostructure for CO_2 reduction.

Photocatalyst	Source of Light	Morphology	Performance	Ref
$ReS_2@Cu_2O/Cu$	300 W Xennon lamp ($\lambda \geq$ 420 nm UV-cutoff filter)	ReS_2 particles on the surface of Cu_2O/Cu frameworks	CO (14.3 µmol h^{-1} g^{-1})	[64]
$Au-Pt/Cu_2O/ReS_2$	300 W Xennon lamp	flower-like microsphere	CH_4 (60.76 µmol h^{-1} g^{-1})	[111]
ReS_2/CdS	visible-light irradiation ($\lambda \geq$ 420 nm)	nanosheets	CO (7.1 µmol h^{-1} g^{-1})	[51]

Chemical modification can adjust the optical and electronic properties of ReS_2 nanosheets and produce new catalytic properties by increasing the catalytic active sites exposed in solution, which is an important goal for the development of practical and efficient solar hydrogen production devices. Wu et al. used C_6H_5COOH on ReS_2 to form a molecular linkage between 2D ReS_2 and 0D two-phase TiO_2 through carboxylate (Figure 5) [56]. This structure provides a Z-scheme molecular electron channel, while the non-functionalized ReS_2 provides an unstable and inefficient type-II path. The ReS_2-C_6H_5COOH-TiO_2 composite photocatalyst can not only provide good wettability, connection, and charge transport for solar hydrogen production but also prevent ReS_2 from being oxidized by photogenerated holes. The composite photocatalyst exhibited high photocatalytic activity for solar hydrogen production (9.5 mmol h^{-1} g^{-1} ReS_2 nanosheets, 4750 times higher than bulk ReS_2) and high cycle stability over 20 h.

4.2. Photocatalytic CO_2 Reduction

Anthropogenic emissions of greenhouse gases, such as CO_2, into the environment can lead to global warming. To reduce CO_2 production, various strategies have been developed. Using clean renewable energy to fix CO_2 can promote the carbon cycle and alleviate the global energy crisis. Therefore, photocatalysis has received extensive attention because it can convert carbon dioxide into renewable fuels. Various photocatalysts have been summarized in Table 2 for the CO_2 reduction.

The valence band edge of ReS_2 (E_V = 1.36 V vs. NHE) is more positive than the oxidation potential of H_2O oxidation (0.82 V vs. NHE at pH = 7), while its conduction band edge (E_C = −0.20 V vs. NHE) is much lower than the reduction potential of CO_2 (−0.52 V vs. NHE at pH = 7), indicating that ReS_2 on its own does not have the ability of photocatalytic reduction of CO_2 [111]. However, the introduction of defects on the ReS_2 surface can not only modulate its band structure but also activate the inert surface to realize efficient charge transfer [51]. For example, Zhang et al. synthesized a type I heterojunction which was composed of ReS_2 nanosheets and CdS nanoparticles via a self-assembly approach (Figure 6a–c). ReS_2 with S vacancies induced by visible-light illumination is beneficial to the chemical adsorption and activation of CO_2, as well as the electron transfer between CO_2 and ReS_2. The optimized ReS_2/CdS heterostructure exhibits an enhanced photocatalytic CO_2-to-CO conversion activity of 7.1 µmol g^{-1} accompanied by a prominent selectivity of 93.4% [51].

Owing to the excellent light absorption, large specific surface area, and abundant active sites of ReS_2, it can serve as an ideal cocatalyst for photocatalytic CO_2 reduction [51,64,111]. Huang et al. constructed an indirect Z-scheme heterostructure $Au-Pt/Cu_2O/ReS_2$ via chemical reduction and photodeposition (Figure 6d,e). The photocatalytic efficiency of the prepared heterojunction was significantly improved, and the CO yield was 30.11 µmol g^{-1}, which was higher than that of pure Cu_2O quantum dots (22.87 µmol g^{-1}). In addition, the selectivity of CH_4 and CO can be controlled by manipulating the mass ratio of Au/Pt (Figure 6f,g). Because of the high work function and excellent conductivity of Au and Pt, the electron transfer was accelerated between Cu_2O and ReS_2 (Figure 6h) [111].
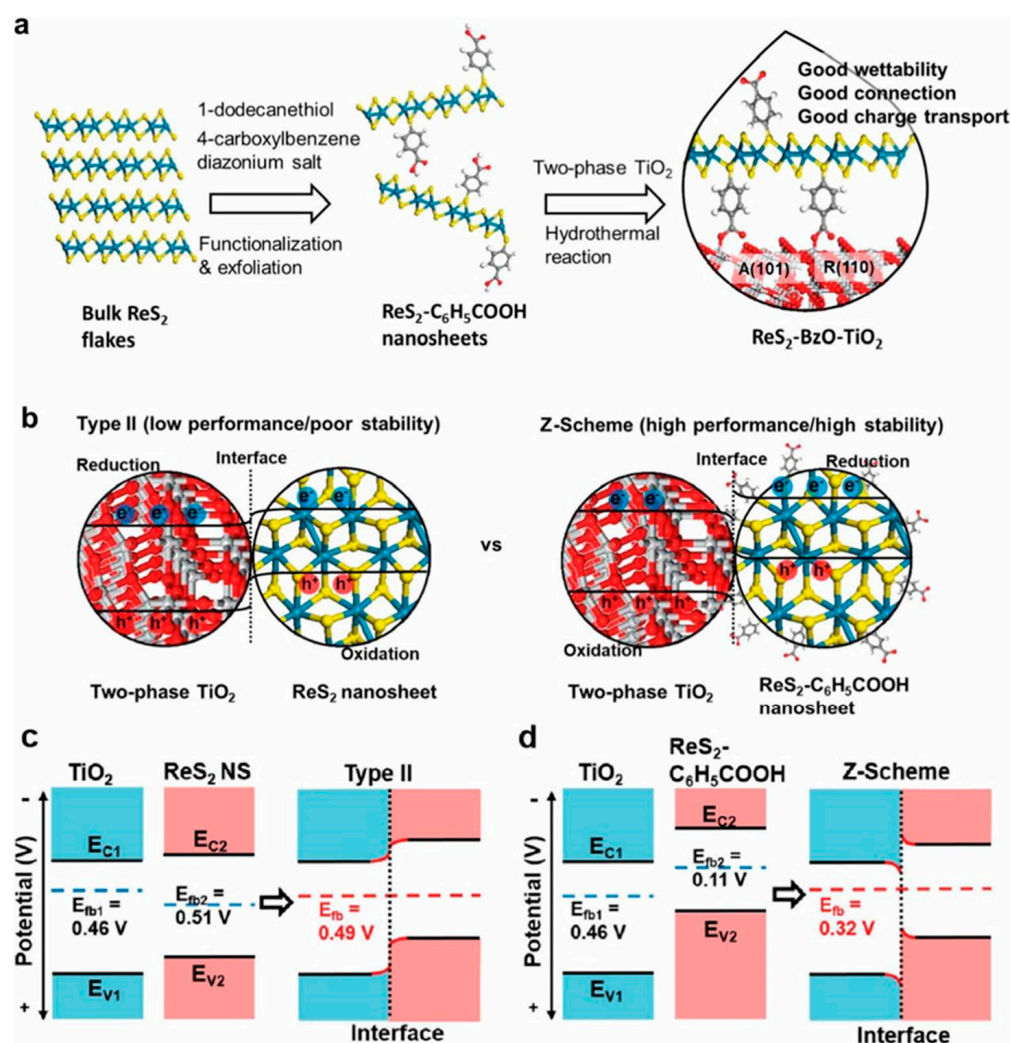
Figure 5. (**a**) Preparation for multiple junctions between functionalized ReS$_2$ nanosheets and two-phase TiO$_2$. (**b**) Proposed transfer paths of photogenerated charges in terms of contact properties at the interface. Type II: The energy bands of TiO$_2$ and nonfunctionalized ReS$_2$ nanosheet can bend upward and downward toward the physically contacted interface, respectively. Z-scheme: The energy bands of TiO$_2$ and ReS$_2$−C$_6$H$_5$COOH can bend downward and upward toward the chemically contacted interface, respectively. (**c**,**d**) Proposed energy band diagrams for ReS$_2$ NS/TiO$_2$ (type II) and ReS$_2$−BzO−TiO$_2$ (Z-scheme) based on the flat-band potentials of each component (E_C—conduction band energy; E_V—valence band energy; E_{fb}—flat-band energy) [56]. Reproduced with permission: Copyright 2020, American Chemical Society.

4.3. Degradation of Organic Pollutants

The increase in energy consumption associated with the rapid development of modern society has led to a corresponding rise in environmental pollution, particularly water pollution, which poses a serious threat to human health and global ecological balance. To address this issue, advanced energy production and pollution control technologies should be developed. Among them, photocatalysts have demonstrated their efficacy in degrading organic pollutants. Various photocatalysts have been summarized in Table 3. Specifically, due to the nonbonding d electron of the Re atom, the 1T-ReS$_2$ phase exhibits a diamond-chain structural distortion caused by the Re−Re bond interaction [112]. Therefore, the transitions of exciton in ReS$_2$ are highly polarization-dependent [113]. More electron–hole pairs and a longer carrier lifetime parallel to the diamond-chain direction give rise to a faster photodegradation rate constant up to 12 times greater than that perpendicular to the diamond-chain direction [114].
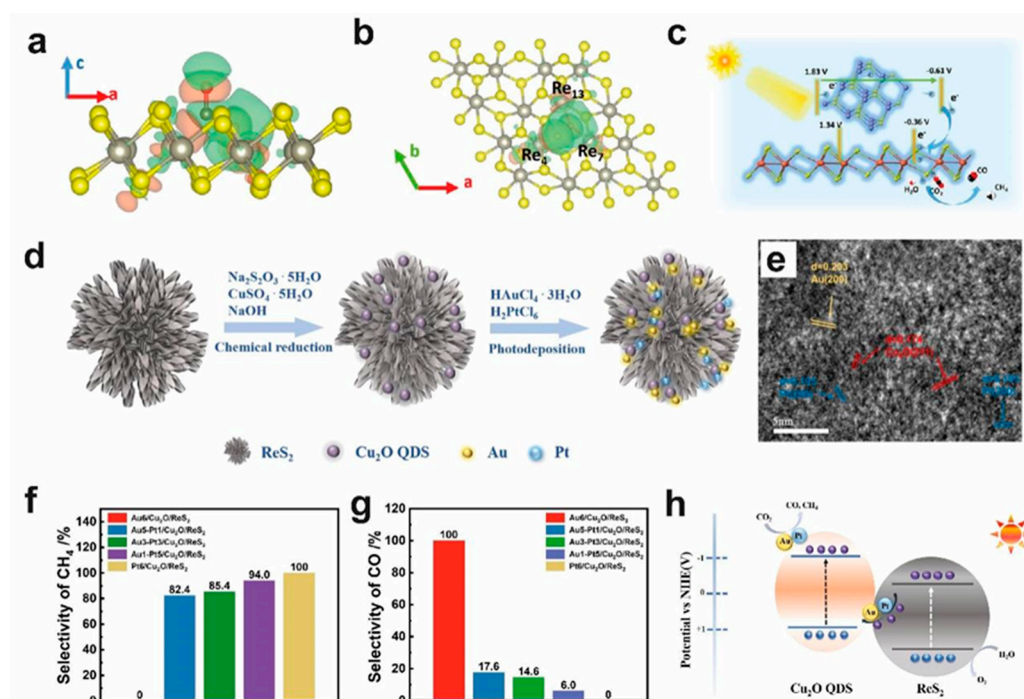
Figure 6. (**a**) Side-view (elevation) and (**b**) top-view (plan) of the electron density distribution of absorbed CO_2 on Vs-ReS_2. (**c**) Schematic of photocatalytic CO_2 reduction in CR12 system under visible-light illumination ($\lambda \geq 420$ nm). The purple-, red-, yellow-, orange-, white-, and black-colored spheres denote Cd, O, S, Re, H, and C atoms, respectively [51]. Reproduced with permission: Copyright 2021, Wiley-VCH Verlag GmbH & Co. KGaA. (**d**) Schematic representation of Au-Pt/Cu_2O/ReS_2 synthesis via the approaches of chemical reduction and photodeposition. (**e**) HRTEM images of Au-Pt/Cu_2O/ReS_2. Selectivity of CH_4 (**f**) and CO (**g**) of Au-Pt/Cu_2O/ReS_2 with different Au-Pt mass ratios. (**h**) Schematic diagram of the transfer processes of the photoexcited electrons and holes and the mechanism of the photocatalytic CO_2 reduction [111]. Copyright 2022, ELSEVIER.

Table 3. Applications of ReS_2-based photocatalysts of pollutants removal.

Photocatalyst	Type	Synthesis Methods	Morphology	Light Source	Application	Efficiency	Cycle	Ref
ReS_2/MIL-88B(Fe)	Type-II	solvothermal method	shuttle structure	Both PS and visible light irradiation	Degradation of Ibuprofen (IBP)	100% (3 h)	3	[52]
TiO_2@ReS_2	Z-scheme	ultrasonic liquid exfoliation method	ReS_2 nanosheets	Solar simulator	Degradation of Rhodamine B (RhB)	94% (120 min)	25	[47]
$BaTiO_3$@ReS_2	Type-I	multi-step hydrothermal method	ReS_2 nanosheets on $BaTiO_3$ nanorods	UV-vis light	Degradation of RhB	96% (25 min)	3	[115]
carbon quantum dots (CQDs)/ReS_2	Type-I	two-step hydrothermal method	rCQDs/ReS_2 nanosheets	300 W Xenon lamp	Cr (VI)	96% (50 min)	6	[86]
ReS_2/Graphite Carbon Nitride (CN)	Type-II	electrostatic assembly process	ReS_2 microspheres and CN nanosheets	300 W Xenon arc lamp ($\lambda \geq 420$ nm cutoff filter)	RhB	94% (30 min)	3	[116]

The construction of a p-n heterojunction can induce a charge diffusion near the interface in nanocomposites until equilibrium is reached at the Fermi level between the two materials. For example, in the TiO_2@ReS_2 nanocomposites, this effect will lift the conduction band position of ReS_2 higher than that of TiO_2, leading to a better electron−hole separation efficiency. Under sunlight irradiation, the degradation activity of organic pigments can be significantly improved compared with pure TiO_2 nanoparticles [47]. Similar strategies take effect such that the ReS_2/MIL-88B(Fe) heterojunction can extend the lifetime of photoexcited electron−hole pairs, absorb more visible light, and enhance persulfate activation, leading to a better catalytic capacity for ibuprofen degradation compared with the individual component [52]. Electrostatic attraction is significant for fabricating heterojunctions. For instance, the g-C_3N_4 and defect-rich ReS_2 attain close contact, resulting in faster generation of the reactive oxygen species than pristine g-C_3N_4 [116].

It is an efficient strategy to improve the photocatalytic performance by constructing a dynamic built-in electric field in a "self-driven" manner to continuously drive the separation of carriers [117]. Recently, a $BaTiO_3$@ReS_2 piezo-assisted photocatalysis heterostructure has been successfully synthesized by Liu et al. [115] through the coupling of interfacial covalent bonds and piezotronics, showing high degradation efficiency for refractory pollutants. The introduction of distorted 1T-ReS_2 can enhance the light absorption of the hybrid nanostructure. Moreover, the formed interfacial Re-O covalent bond (Figure 7a,b) can serve as the channels for charge carriers' transfer. In addition, the internal polarization field in the Schottky interface can reduce the Schottky barrier of photogenerated charge transfer. Consequently, the $BaTiO_3$@ReS_2 system obtained high O_2 activation activity and an excellent synergistic effect under ultrasonic and light conditions. The $BaTiO_3$@ReS_2 exhibits ultrahigh pollutant degradation activity. The apparent rate constant of piezoelectric-assisted photocatalysis is 0.133 min^{-1}, which is 16.6 and 2.44 times that of piezoelectric catalysis and photocatalysis, respectively. (Figure 7c,d) [115].
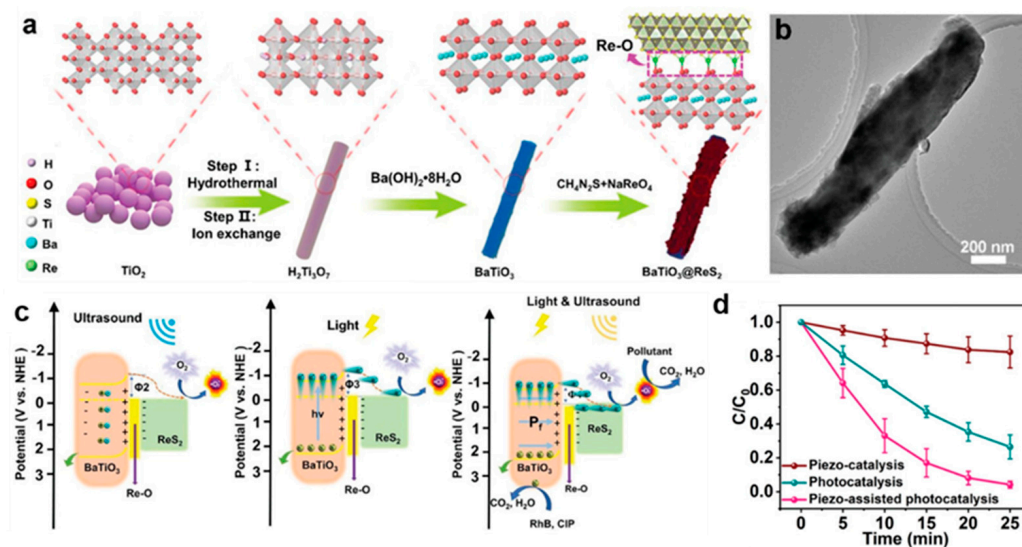

Figure 7. (**a**) Schematic illustration of $BaTiO_3$@ReS_2 system preparation process. (**b**) TEM image of $BaTiO_3$@ReS_2. (**c**) Comparison of the piezo-catalytic, photocatalytic, and piezo-assisted photocatalytic degradation of RhB in the presence of $BaTiO_3$@ReS_2. (**d**) Schematic illustration of the synergy of photocatalysis and piezotronics effects on piezo-assisted photocatalysis system [115]. Reproduced with permission: Copyright 2022, Wiley-VCH Verlag GmbH & Co. KGaA.

4.4. Photocatalytic Reduction of Metal Ions

Heavy metals in aquatic systems and drinking water sources are acutely toxic and carcinogenic to most organisms. Taking Cr (VI) as an example, photocatalytic reduction of Cr (VI) to low-toxic Cr (III) is generally considered to be a promising and practical option because this method is more effective and low-cost and does not produce any

hazardous chemicals. Zhou et al. proposed a simple and feasible atomic hybridization strategy to accelerate the reaction kinetics process via constructing electronic pathways [86]. The reduced carbon quantum dots (rCQDs)/ReS$_2$ heterostructure is synthesized via the CVD and hydrothermal method (Figure 8a,b). Compared with pure ReS$_2$ nanosheets and CQDs/ReS$_2$, the reduction reaction rate constants of the pseudo-first-order kinetic model were increased by about 13.1 and 4.3 times, respectively. (Figure 8c). C=O double bonds reduced and then anchored onto ReS$_2$ nanosheets can form an electronic channel via Re-5d and O-2p orbital hybridization (Figure 8d), in which a photoinduced carrier of the rCQDs can freely migrate to ReS$_2$ for hexavalent chromium reduction (Figure 8e) [86].
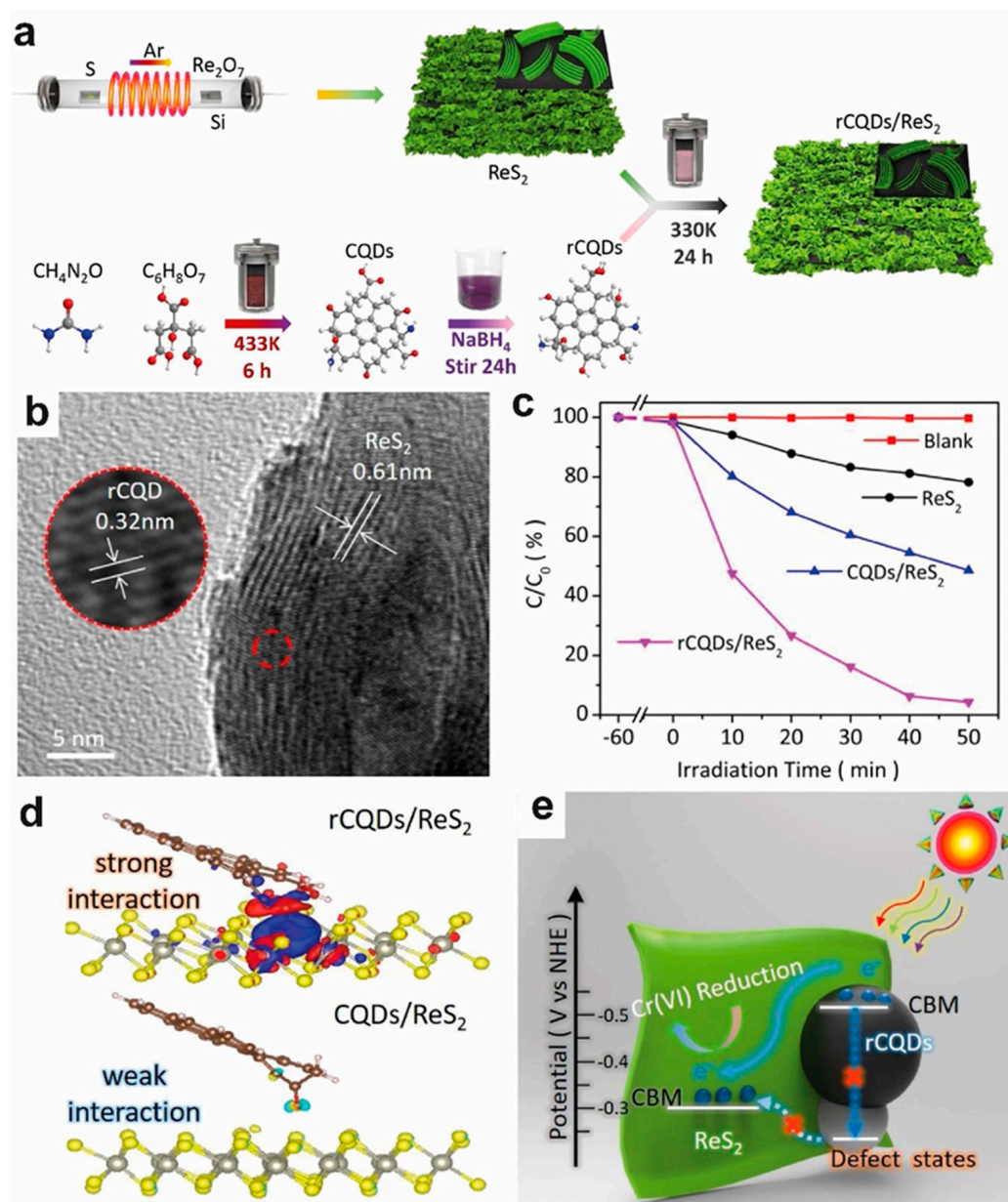

Figure 8. (**a**) Schematic illustration of the preparation process. (**b**) The HR-TEM image of rCQDs/ReS$_2$ heterojunctions. Inset: The corresponding TEM image. (**c**) Reduction curves of the Cr (VI) aqueous solutions containing different photocatalysts under simulated sunlight irradiation: no catalyst, ReS$_2$ nanosheets, CQDs/ReS$_2$ heterojunctions, and rCQDs/ReS$_2$ heterojunctions. (**d**) The charge density difference of rCQD(CQD)/ReS$_2$ heterojunctions. (**e**) Schematic presentation of the carrier transfer process in the rCQD(CQD)/ReS$_2$ heterostructure during reduction [86]. Reproduced with permission: Copyright 2022, ELSEVIER.

4.5. Photocatalytic Water Disinfection

　　　The treatment cost of freshwater pollution is high, and the shortage of freshwater resources has become a more complex problem. Photocatalysis techniques have been regarded as one of the most promising strategies for environmental remediation. It is well known that when the photocatalyst absorbs light, electron−hole pairs are formed, which interact with water and dissolved oxygen to generate activated oxygen species (ROS), such as hydroxyl radicals, singlet oxygen, and superoxide [118]. These strong oxidants can destroy essential macromolecules in bacteria, resulting in bacterial disinfection [119]. The field of ReS_2 photocatalytic sterilization is still in the preliminary stages. Pioneer work by Ghoshal et al. proved that vertically oriented ReS_2 nanosheets show great potential for photocatalytic water disinfection [78]. However, due to the rapid recombination of the carriers, its inactivation efficiency still needs to be further enhanced.

　　　It has been found that the construction of a 0D/2D heterostructure can greatly improve the sterilization efficiency of a photocatalyst because of the effective separation of charge carriers. Recently, Zhang et al. have reported that a Ag-modified ReS_2 heterostructure grown on a series of substrates can be used as a visible-light-driven photocatalyst for highly efficient water sterilization. Different substrates and the size of Ag nanoparticles are critical to the photocatalytic bactericidal performance (Figure 9a,b). The Ag nanoparticles on the surface of ReS_2 nanosheets can not only act as electron capture agents to promote the separation of photogenerated carriers but also inhibit the recombination of photogenerated carriers (Figure 9c). The main active substances in the photocatalysis process are h^+, $\bullet OH$, and $\bullet O^{2-}$. All *Escherichia coli* can be inactivated within 30 min at a concentration of 1.72 mg L^{-1} by the reusable Ag/ReS_2 heterostructure under visible light irradiation (Figure 9d) [85].
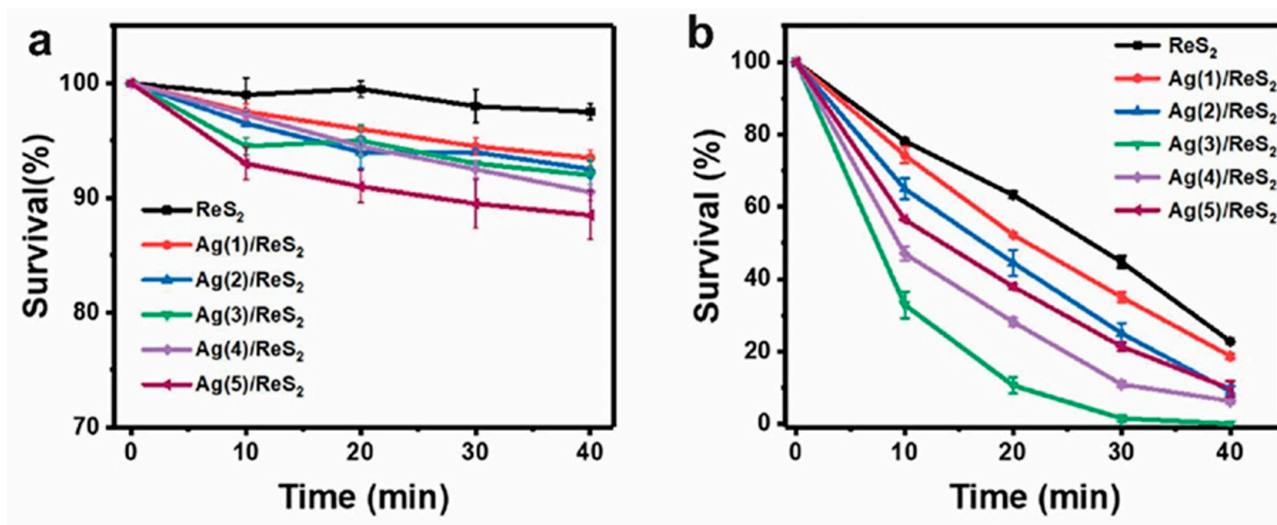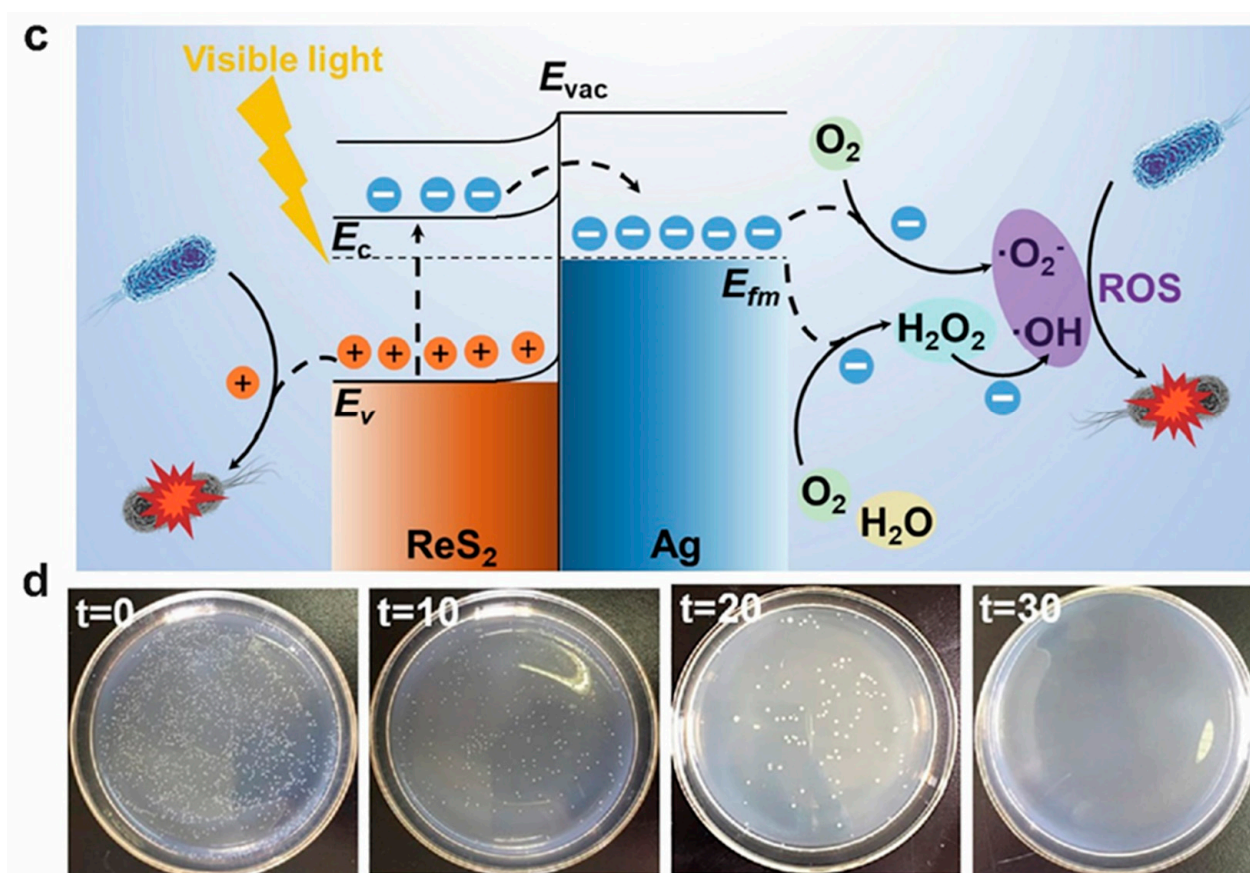

Figure 9. *Cont.*

Figure 9. Photocatalytic sterilization efficiency to *Escherichia coli* of different Ag-content samples grown on porous carbon cloth substrate, (**a**) under dark condition, (**b**) under visible light. (**c**) Schematic illustration of charge separation and photocatalytic disinfection via reactive oxygen species (ROS). (**d**) Photos of *Escherichia coli* colonies corresponding to photocatalytic sterilization for 0 min, 10 min, 20 min, and 30 min [85]. Reproduced with permission: Copyright 2022, ELSEVIER.

5. Summary and Outlook

Two-dimensional ReS_2, a special new material in the family of TMDs, has great potential as a photocatalyst due to its favorable band structure, which is independent of the number of layers, as well as its high specific surface area and numerous active sites. This review summarizes the basic properties and heterostructure synthesis methods of ReS_2. Several types of ReS_2-based heterostructures and their recent progress in photocatalysis fields, such as photocatalytic hydrogen production, CO_2 reduction, and pollutant degradation, are then reviewed, demonstrating that ReS_2 is an efficient and stable photocatalyst. However, the research on ReS_2 is still in its early stages, and there is room for improvement of its photocatalytic performance. Based on synthetic chemical mechanisms, semiconductor physics of photocatalysis, and recent research results, the following aspects can be further explored for the rational design of efficient heterostructure photocatalysts:

1. Developing new synthetic methodologies to achieve precise synthesis of ReS_2 and its composites. Mechanical mixing is usually used in the construction of heterojunctions for ReS_2, but precise design for the interactions between the two or more materials has not yet been realized in the preparation of photocatalysts, resulting in random morphology and exposed crystal faces of the composites. With the growth mechanism of ReS_2 as a basis, rational control of the growth conditions is expected to precisely control the size and crystal face orientation. In addition, reducing the size of ReS_2 down to sub-10-nanometers is another intriguing direction due to the enhanced quantum confinement effect and derived novel photonic properties; however, structural

2. controllability including particle diameter, edge structure, phase transition, etc. is highly important and is also well deserving of more research attention.

2. Surface engineering strategies toward tailorable physicochemical properties of ReS_2. Few studies on the design and modification of the surface structure of ReS_2 have been reported for photocatalytic research. Surface defects can become centers of the electron−hole complex, but they are not entirely inutile. For example, introducing Re vacancies in a reasonable way can enhance the adsorption ability of H^+. In addition, organic molecules can form chemical bonds on the surface S vacancies, which can improve the interface wettability of ReS_2 on the one hand and fine-tune its energy band position on the other hand.

3. Combining novel characterization methods with theoretical calculations. The surface and interface structure changes in photocatalysis should be thoroughly investigated from both microscopic and transient aspects. Real-time monitoring of intermediates and catalytic products is essential for understanding the photocatalytic mechanism and further optimizing the performance of photocatalysts. For instance, in situ Fourier Transform Infrared spectroscopy and online mass spectrometry can probe the source of hydrogen and the fate of the sacrifice reagents in photocatalytic hydrogen evolution [59]. Ultra-high spatial and temporal resolution technique, such as tip-enhanced Raman spectroscopy, can greatly improve the signal-to-noise ratio and spatial resolution, allowing for the characterization of single molecules and even single chemical bonds. Moreover, the theoretical simulation of the model systems, particularly first-principles, external field simulations, and micro-reaction dynamics simulations, is essential for exploring the fundamental mechanisms of photocatalysis. The binding energy between various intermediates and catalysts can be obtained by calculating the adsorption energy and charge density difference, further reflecting the configuration of the reaction intermediates on the catalyst surface.

Overall, ReS_2 has the potential to excel as a photocatalytic material, and further investigation into its photocatalytic performance and mechanism could propel the development of photocatalysis and provide new insights into environmental and energy issues.

Institutional Review Board Statement: Not applicable.

Informed Consent Statement: Not applicable.

Data Availability Statement: Data are contained within the article.

Conflicts of Interest: The authors declare no conflict of interest.

References

1. Tian, J.; Zhao, Z.; Kumar, A.; Boughton, R.I.; Liu, H. Recent progress in design, synthesis, and applications of one-dimensional TiO_2 nanostructured surface heterostructures: A review. *Chem. Soc. Rev.* **2014**, *43*, 6920–6937. [CrossRef] [PubMed]
2. Fujishima, A.; Honda, K. Electrochemical Photolysis of Water at a Semiconductor Electrode. *Nature* **1972**, *238*, 37–38. [CrossRef] [PubMed]
3. Du, J.; Lai, X.; Yang, N.; Zhai, J.; Kisailus, D.; Su, F.; Wang, D.; Jiang, L. Hierarchically Ordered Macro−Mesoporous TiO_2−Graphene Composite Films: Improved Mass Transfer, Reduced Charge Recombination, and Their Enhanced Photocatalytic Activities. *ACS Nano* **2011**, *5*, 590–596. [CrossRef]
4. Khan, M.M.; Ansari, S.A.; Pradhan, D.; Ansari, M.O.; Han, D.H.; Lee, J.; Cho, M.H. Band gap engineered TiO_2 nanoparticles for visible light induced photoelectrochemical and photocatalytic studies. *J. Mater. Chem. A* **2014**, *2*, 637–644. [CrossRef]

5.   Katal, R.; Salehi, M.; Davood Abadi Farahani, M.H.; Masudy-Panah, S.; Ong, S.L.; Hu, J. Preparation of a New Type of Black TiO$_2$ under a Vacuum Atmosphere for Sunlight Photocatalysis. *ACS Appl. Mater. Interfaces* **2018**, *10*, 35316–35326. [CrossRef] [PubMed]

6.   Yang, Y.; Ye, K.; Cao, D.; Gao, P.; Qiu, M.; Liu, L.; Yang, P. Efficient Charge Separation from F– Selective Etching and Doping of Anatase-TiO$_2${001} for Enhanced Photocatalytic Hydrogen Production. *ACS Appl. Mater. Interfaces* **2018**, *10*, 19633–19638. [CrossRef]

7.   Tong, H.; Ouyang, S.; Bi, Y.; Umezawa, N.; Oshikiri, M.; Ye, J. Nano-photocatalytic Materials: Possibilities and Challenges. *Adv. Mater.* **2012**, *24*, 229–251. [CrossRef]

8.   Zhang, C.; Zhou, Y.; Bao, J.; Sheng, X.; Fang, J.; Zhao, S.; Zhang, Y.; Chen, W. Hierarchical Honeycomb Br-, N-Codoped TiO$_2$ with Enhanced Visible-Light Photocatalytic H$_2$ Production. *ACS Appl. Mater. Interfaces* **2018**, *10*, 18796–18804. [CrossRef]

9.   Bian, Z.; Tachikawa, T.; Zhang, P.; Fujitsuka, M.; Majima, T. Au/TiO$_2$ Superstructure-Based Plasmonic Photocatalysts Exhibiting Efficient Charge Separation and Unprecedented Activity. *J. Am. Chem. Soc.* **2014**, *136*, 458–465. [CrossRef]

10. Yang, R.; Fan, Y.; Zhang, Y.; Mei, L.; Zhu, R.; Qin, J.; Hu, J.; Chen, Z.; Hau Ng, Y.; Voiry, D.; et al. 2D Transition Metal Dichalcogenides for Photocatalysis. *Angew. Chem. Int. Ed.* **2023**, *62*, e202218016. [CrossRef]

11. Faraji, M.; Yousefi, M.; Yousefzadeh, S.; Zirak, M.; Naseri, N.; Jeon, T.H.; Choi, W.; Moshfegh, A.Z. Two-dimensional materials in semiconductor photoelectrocatalytic systems for water splitting. *Energy Environ. Sci.* **2019**, *12*, 59–95. [CrossRef]

12. Tong, R.; Ng, K.W.; Wang, X.; Wang, S.; Wang, X.; Pan, H. Two-dimensional materials as novel co-catalysts for efficient solar-driven hydrogen production. *J. Mater. Chem. A* **2020**, *8*, 23202–23230. [CrossRef]

13. Lotsch, B.V. Vertical 2D Heterostructures. *Annu. Rev. Mater. Res.* **2015**, *45*, 85–109. [CrossRef]

14. Chhowalla, M.; Shin, H.S.; Eda, G.; Li, L.J.; Loh, K.P.; Zhang, H. The chemistry of two-dimensional layered transition metal dichalcogenide nanosheets. *Nat. Chem.* **2013**, *5*, 263–275. [CrossRef] [PubMed]

15. Mak, K.F.; Lee, C.; Hone, J.; Shan, J.; Heinz, T.F. Atomically Thin MoS$_2$: A New Direct-Gap Semiconductor. *Phys. Rev. Lett.* **2010**, *105*, 136805. [CrossRef]

16. Fu, Q.; Han, J.; Wang, X.; Xu, P.; Yao, T.; Zhong, J.; Zhong, W.; Liu, S.; Gao, T.; Zhang, Z.; et al. 2D Transition Metal Dichalcogenides: Design, Modulation, and Challenges in Electrocatalysis. *Adv. Mater.* **2021**, *33*, e1907818. [CrossRef]

17. Pi, L.; Li, L.; Liu, K.; Zhang, Q.; Li, H.; Zhai, T. Recent Progress on 2D Noble-Transition-Metal Dichalcogenides. *Adv. Funct. Mater.* **2019**, *29*, 1904932. [CrossRef]

18. Wu, E.; Xie, Y.; Wang, S.; Zhang, D.; Hu, X.; Liu, J. Multi-level flash memory device based on stacked anisotropic ReS$_2$-boron nitride-graphene heterostructures. *Nanoscale* **2020**, *12*, 18800–18806. [CrossRef]

19. Mukherjee, B.; Hayakawa, R.; Watanabe, K.; Taniguchi, T.; Nakaharai, S.; Wakayama, Y. ReS$_2$/h-BN/Graphene Heterostructure Based Multifunctional Devices: Tunneling Diodes, FETs, Logic Gates, and Memory. *Adv. Electron. Mater.* **2021**, *7*, 2000925. [CrossRef]

20. Qin, J.-K.; Qiu, G.; He, W.; Jian, J.; Si, M.-W.; Duan, Y.-Q.; Charnas, A.; Zemlyanov, D.Y.; Wang, H.-Y.; Shao, W.-Z.; et al. Epitaxial Growth of 1D Atomic Chain Based Se Nanoplates on Monolayer ReS$_2$ for High-Performance Photodetectors. *Adv. Funct. Mater.* **2018**, *28*, 1806254. [CrossRef]

21. Varghese, A.; Saha, D.; Thakar, K.; Jindal, V.; Ghosh, S.; Medhekar, N.V.; Ghosh, S.; Lodha, S. Near-Direct Bandgap WSe$_2$/ReS$_2$ Type-II pn Heterojunction for Enhanced Ultrafast Photodetection and High-Performance Photovoltaics. *Nano Lett.* **2020**, *20*, 1707–1717. [CrossRef] [PubMed]

22. Ma, H.; Xing, Y.; Han, J.; Cui, B.; Lei, T.; Tu, H.; Guan, B.; Zeng, Z.; Zhang, B.; Lv, W. Ultrasensitive and Broad-Spectrum Photodetectors Based on InSe/ReS$_2$ Heterostructure. *Adv. Opt. Mater.* **2022**, *10*, 2101772. [CrossRef]

23. Su, W.; Zhang, S.; Liu, C.; Tian, Q.; Liu, X.; Li, K.; Lv, Y.; Liao, L.; Zou, X. Interlayer Transition Induced Infrared Response in ReS$_2$/2D Perovskite van der Waals Heterostructure Photodetector. *Nano Lett.* **2022**, 10192–10199. [CrossRef] [PubMed]

24. Tran, T.U.; Bahng, J.; Dang, X.D.; Oh, S.; Duong, H.P.; Kang, S.S.; Yu, H.M.; Sakong, W.; Kim, M.; Choi, H.-S.; et al. Adaptive photocurrent generation of ReS$_2$-2D Te heterostructure. *Nano Energy* **2022**, *102*, 107720. [CrossRef]

25. Liu, Y.; Zhang, H.; Song, W.; Zhang, Y.; Hou, Z.; Zhou, G.; Zhang, Z.; Liu, J. In-situ growth of ReS$_2$/NiS heterostructure on Ni foam as an ultra-stable electrocatalyst for alkaline hydrogen generation. *Chem. Eng. J.* **2023**, *451*, 138905. [CrossRef]

26. Zhou, G.; Guo, Z.; Shan, Y.; Wu, S.; Zhang, J.; Yan, K.; Liu, L.; Chu, P.K.; Wu, X. High-efficiency hydrogen evolution from seawater using hetero-structured T/Td phase ReS$_2$ nanosheets with cationic vacancies. *Nano Energy* **2019**, *55*, 42–48. [CrossRef]

27. Ng, S.; Iffelsberger, C.; Sofer, Z.; Pumera, M. Tunable Room-Temperature Synthesis of ReS$_2$ Bicatalyst on 3D- and 2D-Printed Electrodes for Photo- and Electrochemical Energy Applications. *Adv. Funct. Mater.* **2020**, *30*, 1910193. [CrossRef]

28. Cheng, P.; Liu, Y.; Ziegler, M.; Klingenhof, M.; Wang, D.; Zhang, Z.; Strasser, P.; Schaaf, P. Improving Silicon Photocathode Performance for Water Reduction through Dual Interface Engineering and Integrating ReS$_2$ Photocatalyst. *ACS Appl. Energy Mater.* **2022**, *5*, 8222–8231. [CrossRef]

29. Tongay, S.; Sahin, H.; Ko, C.; Luce, A.; Fan, W.; Liu, K.; Zhou, J.; Huang, Y.-S.; Ho, C.-H.; Yan, J.; et al. Monolayer behaviour in bulk ReS$_2$ due to electronic and vibrational decoupling. *Nat. Commun.* **2014**, *5*, 3252. [CrossRef]

30. Lin, Y.-C.; Komsa, H.-P.; Yeh, C.-H.; Björkman, T.; Liang, Z.-Y.; Ho, C.-H.; Huang, Y.-S.; Chiu, P.-W.; Krasheninnikov, A.V.; Suenaga, K. Single-Layer ReS$_2$: Two-Dimensional Semiconductor with Tunable In-Plane Anisotropy. *ACS Nano* **2015**, *9*, 11249–11257. [CrossRef]

31. Feng, Y.; Zhou, W.; Wang, Y.; Zhou, J.; Liu, E.; Fu, Y.; Ni, Z.; Wu, X.; Yuan, H.; Miao, F.; et al. Raman vibrational spectra of bulk to monolayer ReS$_2$ with lower symmetry. *Phys. Rev. B* **2015**, *92*, 054110. [CrossRef]

32. Rahman, M.; Davey, K.; Qiao, S.Z. Advent of 2D Rhenium Disulfide (ReS$_2$): Fundamentals to Applications. *Adv. Funct. Mater.* **2017**, *27*, 1606129. [CrossRef]

33. Zhang, Q.; Wang, W.; Zhang, J.; Zhu, X.; Zhang, Q.; Zhang, Y.; Ren, Z.; Song, S.; Wang, J.; Ying, Z.; et al. Highly Efficient Photocatalytic Hydrogen Evolution by ReS$_2$ via a Two-Electron Catalytic Reaction. *Adv. Mater.* **2018**, *30*, e1707123. [CrossRef] [PubMed]

34. Ran, J.; Zhang, H.; Qu, J.; Shan, J.; Chen, S.; Yang, F.; Zheng, R.; Cairney, J.; Song, L.; Jing, L.; et al. Atomic-Level Insights into the Edge Active ReS$_2$ Ultrathin Nanosheets for High-Efficiency Light-to-Hydrogen Conversion. *ACS Mater. Lett.* **2020**, *2*, 1484–1494. [CrossRef]

35. Zhang, Q.; Fu, L. Novel Insights and Perspectives into Weakly Coupled ReS$_2$ toward Emerging Applications. *Chem* **2019**, *5*, 505–525. [CrossRef]

36. Cao, Y.-D.; Sun, Y.-H.; Shi, S.-F.; Wang, R.-M. Anisotropy of two-dimensional ReS$_2$ and advances in its device application. *Rare Met.* **2021**, *40*, 3357–3374. [CrossRef]

37. Xie, X.; Mao, M.; Qi, S.; Ma, J. ReS$_2$-Based electrode materials for alkali-metal ion batteries. *CrystEngComm* **2019**, *21*, 3755–3769. [CrossRef]

38. Xiong, Y.; Chen, H.; Zhang, D.W.; Zhou, P. Electronic and Optoelectronic Applications Based on ReS$_2$. *Phys. Status Solidi Rapid Res. Lett.* **2019**, *13*, 1800658. [CrossRef]

39. Fadhel, M.M.; Ali, N.; Rashid, H.; Sapiee, N.M.; Hamzah, A.E.; Zan, M.S.D.; Aziz, N.A.; Arsad, N. A Review on Rhenium Disulfide: Synthesis Approaches, Optical Properties, and Applications in Pulsed Lasers. *Nanomaterials* **2021**, *11*, 2367. [CrossRef]

40. Ren, H.; Xiang, G. Recent Progress in Research on Ferromagnetic Rhenium Disulfide. *Nanomaterials* **2022**, *12*, 3451. [CrossRef]

41. Wang, X.; Wang, X.; Huang, J.; Li, S.; Meng, A.; Li, Z. Interfacial chemical bond and internal electric field modulated Z-scheme Sv-ZnIn$_2$S$_4$/MoSe$_2$ photocatalyst for efficient hydrogen evolution. *Nat. Commun.* **2021**, *12*, 4112. [CrossRef] [PubMed]

42. Zhao, D.; Wang, Y.; Dong, C.-L.; Huang, Y.-C.; Chen, J.; Xue, F.; Shen, S.; Guo, L. Boron-doped nitrogen-deficient carbon nitride-based Z-scheme heterostructures for photocatalytic overall water splitting. *Nat. Energy* **2021**, *6*, 388–397. [CrossRef]

43. Xi, Y.; Wang, F.; Feng, H.; Xiong, Y.; Huang, Q. Cauliflower-like Mn$_{0.2}$Cd$_{0.8}$S decorated with ReS$_2$ nanosheets for boosting photocatalytic H$_2$ evolution activity. *New J. Chem.* **2021**, *45*, 15949–15955. [CrossRef]

44. Ma, X.; Cheng, H. ReS$_2$ with unique trion behavior as a co-catalyst for enhanced sunlight hydrogen production. *J. Colloid Interface Sci.* **2022**, *634*, 32–43. [CrossRef] [PubMed]

45. Liu, J.; Chen, K.; Pan, G.M.; Luo, Z.J.; Xie, Y.; Li, Y.Y.; Lin, Y.J.; Hao, Z.H.; Zhou, L.; Ding, S.J.; et al. Largely enhanced photocatalytic hydrogen production rate of CdS/(Au-ReS$_2$) nanospheres by the dielectric-plasmon hybrid antenna effect. *Nanoscale* **2018**, *10*, 19586–19594. [CrossRef]

46. Xing, C.; Zhao, H.; Yu, G.; Guo, L.; Hu, Y.; Chen, T.; Jiang, L.; Li, X. Modification of g-C$_3$N$_4$ Photocatalyst with Flower-like ReS$_2$ for Highly Efficient Photocatalytic Hydrogen Evolution. *ChemCatChem* **2020**, *12*, 6385–6392. [CrossRef]

47. Jing, Q.; Zhang, H.; Huang, H.; Fan, X.; Zhang, Y.; Hou, X.; Xu, Q.; Ni, Z.; Qiu, T. Ultrasonic exfoliated ReS$_2$ nanosheets: Fabrication and use as co-catalyst for enhancing photocatalytic efficiency of TiO$_2$ nanoparticles under sunlight. *Nanotechnology* **2019**, *30*, 184001. [CrossRef] [PubMed]

48. Fujita, T.; Ito, Y.; Tan, Y.; Yamaguchi, H.; Hojo, D.; Hirata, A.; Voiry, D.; Chhowalla, M.; Chen, M. Chemically exfoliated ReS$_2$ nanosheets. *Nanoscale* **2014**, *6*, 12458–12462. [CrossRef]

49. Yu, Z.G.; Cai, Y.; Zhang, Y.-W. Robust Direct Bandgap Characteristics of One- and Two-Dimensional ReS$_2$. *Sci. Rep.* **2015**, *5*, 13783. [CrossRef]

50. Ran, J.; Zhang, H.; Qu, J.; Shan, J.; Davey, K.; Cairney, J.M.; Jing, L.; Qiao, S.Z. Significantly Raised Visible-Light Photocatalytic H$_2$ Evolution on a 2D/2D ReS$_2$/In$_2$ZnS$_4$ van der Waals Heterostructure. *Small* **2021**, *17*, 2100296. [CrossRef]

51. Zhang, Y.; Yao, D.; Xia, B.; Xu, H.; Tang, Y.; Davey, K.; Ran, J.; Qiao, S.-Z. ReS$_2$ Nanosheets with In Situ Formed Sulfur Vacancies for Efficient and Highly Selective Photocatalytic CO$_2$ Reduction. *Small Sci.* **2021**, *1*, 2000052. [CrossRef]

52. Liu, N.; Dai, W.; Fei, F.; Xu, H.; Lei, J.; Quan, G.; Zheng, Y.; Zhang, X.; Tang, L. Insights into the photocatalytic activation persulfate by visible light over ReS$_2$/MIL-88B(Fe) for highly efficient degradation of ibuprofen: Combination of experimental and theoretical study. *Sep. Purif. Technol.* **2022**, *297*, 121545. [CrossRef]

53. Zhan, X.; Ou, D.; Zheng, Y.; Li, B.; Xu, L.; Yang, H.; Yang, W.; Zhang, H.; Hou, H.; Yang, W. Boosted photocatalytic hydrogen production over two-dimensional/two-dimensional Ta$_3$N$_5$/ReS$_2$ van der Waals heterojunctions. *J. Colloid Interface Sci.* **2023**, *629*, 455–466. [CrossRef] [PubMed]

54. Yang, T.; Shao, Y.; Hu, J.; Qu, J.; Yang, X.; Yang, F.; Ming Li, C. Ultrathin layered 2D/2D heterojunction of ReS$_2$/high-crystalline g-C$_3$N$_4$ for significantly improved photocatalytic hydrogen evolution. *Chem. Eng. J.* **2022**, *448*, 137613. [CrossRef]

55. Knirsch, K.C.; Berner, N.C.; Nerl, H.C.; Cucinotta, C.S.; Gholamvand, Z.; McEvoy, N.; Wang, Z.; Abramovic, I.; Vecera, P.; Halik, M.; et al. Basal-Plane Functionalization of Chemically Exfoliated Molybdenum Disulfide by Diazonium Salts. *ACS Nano* **2015**, *9*, 6018–6030. [CrossRef] [PubMed]

56. Yu, J.; Seo, S.; Luo, Y.; Sun, Y.; Oh, S.; Nguyen, C.T.K.; Seo, C.; Kim, J.H.; Kim, J.; Lee, H. Efficient and Stable Solar Hydrogen Generation of Hydrophilic Rhenium-Disulfide-Based Photocatalysts via Chemically Controlled Charge Transfer Paths. *ACS Nano* **2020**, *14*, 1715–1726. [CrossRef]

57. Wang, X.; Xue, Y.; Liang, Z.; Tian, J.; Zhang, X.; Chen, X. Insights into the function of semi-metallic 1T' phase ReS$_2$ as cocatalyst decorated g-C$_3$N$_4$ nanotubes for enhanced photocatalytic hydrogen production activity. *Mater. Today Adv.* **2022**, *15*, 100257. [CrossRef]

58. Wang, X.; Chen, B.; Yan, D.; Zhao, X.; Wang, C.; Liu, E.; Zhao, N.; He, F. Distorted 1T-ReS$_2$ Nanosheets Anchored on Porous TiO$_2$ Nanofibers for Highly Enhanced Photocatalytic Hydrogen Production. *ACS Appl. Mater. Interfaces* **2019**, *11*, 23144–23151. [CrossRef]

59. Ye, L.; Ma, Z.; Deng, Y.; Ye, Y.; Li, W.; Kou, M.; Xie, H.; Zhikun, X.; Zhou, Y.; Xia, D.; et al. Robust and efficient photocatalytic hydrogen generation of ReS$_2$/CdS and mechanistic study by on-line mass spectrometry and in situ infrared spectroscopy. *Appl. Catal. B* **2019**, *257*, 117897. [CrossRef]

60. Zhan, X.; Fang, Z.; Li, B.; Zhang, H.; Xu, L.; Hou, H.; Yang, W. Rationally designed Ta$_3$N$_5$@ReS$_2$ heterojunctions for promoted photocatalytic hydrogen production. *J. Mater. Chem. A* **2021**, *9*, 27084–27094. [CrossRef]

61. Xiong, X.; Yan, A.; Zhang, X.; Huang, F.; Li, Z.; Zhang, Z.; Weng, H. ReS$_2$/ZnIn$_2$S$_4$ heterojunctions with enhanced visible-light-driven hydrogen evolution performance for water splitting. *J. Alloys Compd.* **2021**, *873*, 159850. [CrossRef]

62. Chen, R.; Ma, M.; Luo, Y.; Qian, L.; Xu, S. Enhanced interfacial effect between CdS and ReS$_2$ on boosted hydrogen evolution performance via phase structure engineering. *J. Solid State Chem.* **2022**, *312*, 123238. [CrossRef]

63. Song, T.; Wang, J.; Su, L.; Xu, H.; Bai, X.; Zhou, L.; Tu, W. Promotion effect of rhenium on MoS$_2$/ReS$_2$@CdS nanostructures for photocatalytic hydrogen production. *Mol. Catal.* **2021**, *516*, 111939. [CrossRef]

64. Liu, J.; Qi, F.; Zhang, N.; Yang, J.; Liang, Z.; Tian, C.; Zhang, W.; Tang, X.; Wu, D.; Huang, Q. Three-dimensional structural ReS$_2$@Cu$_2$O/Cu heterojunction photocatalysts for visible-light-driven CO$_2$ reduction. *J. Mater. Sci.* **2022**, *57*, 15474–15487. [CrossRef]

65. Zhang, L.; Zheng, Q.; Xie, Y.; Lan, Z.; Prezhdo, O.V.; Saidi, W.A.; Zhao, J. Delocalized Impurity Phonon Induced Electron-Hole Recombination in Doped Semiconductors. *Nano Lett.* **2018**, *18*, 1592–1599. [CrossRef] [PubMed]

66. Ji, Q.; Zhang, Y.; Zhang, Y.; Liu, Z. Chemical vapour deposition of group-VIB metal dichalcogenide monolayers: Engineered substrates from amorphous to single crystalline. *Chem. Soc. Rev.* **2015**, *44*, 2587–2602. [CrossRef] [PubMed]

67. Shi, Y.; Li, H.; Li, L.-J. Recent advances in controlled synthesis of two-dimensional transition metal dichalcogenides via vapour deposition techniques. *Chem. Soc. Rev.* **2015**, *44*, 2744–2756. [CrossRef]

68. Zereshki, P.; Yao, P.; He, D.; Wang, Y.; Zhao, H. Interlayer charge transfer in ReS$_2$/WS$_2$ van der Waals heterostructures. *Phys. Rev. B* **2019**, *99*, 195438. [CrossRef]

69. Varghese, A.; Joseph, D.; Ghosh, S.; Thakar, K.; Mcdhckar, N.; Lodha, S. WSe2/ReS2 vdW Heterostructure for Versatile Optoelectronic Applications. In Proceedings of the 2018 76th Device Research Conference (DRC), Santa Barbara, CA, USA, 24–27 June 2018.

70. Wei, N.; Cai, J.; Wang, R.; Wang, M.; Lv, W.; Ci, H.; Sun, J.; Liu, Z. Elevated polysulfide regulation by an ultralight all-CVD-built ReS$_2$@N-Doped graphene heterostructure interlayer for lithium-sulfur batteries. *Nano Energy.* **2019**, *66*, 104190.

71. Li, J.; Song, P.; Zhao, J.; Vaklinova, K.; Zhao, X.; Li, Z.; Qiu, Z.; Wang, Z.; Lin, L.; Zhao, M.; et al. Printable two-dimensional superconducting monolayers. *Nat. Mater.* **2021**, *20*, 181–187.

72. Liu, D.; Hong, J.; Li, X.; Zhou, X.; Jin, B.; Cui, Q.; Chen, J.; Feng, Q.; Xu, C.; Zhai, T.; et al. Synthesis of 2H-1T' WS$_2$-ReS$_2$ Heterophase Structures with Atomically Sharp Interface via Hydrogen-Triggered One-Pot Growth. *Adv. Funct. Mater.* **2020**, *30*, 1910169. [CrossRef]

73. Chen, B.; Wu, K.; Suslu, A.; Yang, S.; Cai, H.; Yano, A.; Soignard, E.; Aoki, T.; March, K.; Shen, Y.; et al. Controlling Structural Anisotropy of Anisotropic 2D Layers in Pseudo-1D/2D Material Heterojunctions. *Adv. Mater.* **2017**, *29*, 1701201. [CrossRef] [PubMed]

74. Liu, D.; Hong, J.; Wang, X.; Li, X.; Feng, Q.; Tan, C.; Zhai, T.; Ding, F.; Peng, H.; Xu, H. Diverse Atomically Sharp Interfaces and Linear Dichroism of 1T' ReS$_2$-ReSe$_2$ Lateral p–n Heterojunctions. *Adv. Funct. Mater.* **2018**, *28*, 1804696. [CrossRef]

75. Zhang, T.; Jiang, B.; Xu, Z.; Mendes, R.G.; Xiao, Y.; Chen, L.; Fang, L.; Gemming, T.; Chen, S.; Rummeli, M.H.; et al. Twinned growth behaviour of two-dimensional materials. *Nat. Commun.* **2016**, *7*, 13911. [CrossRef]

76. Lim, J.; Kadyrov, A.; Jeon, D.; Choi, Y.; Bae, J.; Lee, S. Contact Engineering of Vertically Grown ReS$_2$ with Schottky Barrier Modulation. *ACS Appl. Mater. Interfaces* **2021**, *13*, 7529–7538. [CrossRef]

77. Zhou, J.; Lin, J.; Huang, X.; Zhou, Y.; Chen, Y.; Xia, J.; Wang, H.; Xie, Y.; Yu, H.; Lei, J.; et al. A library of atomically thin metal chalcogenides. *Nature* **2018**, *556*, 355–359. [CrossRef]

78. Ghoshal, D.; Yoshimura, A.; Gupta, T.; House, A.; Basu, S.; Chen, Y.; Wang, T.; Yang, Y.; Shou, W.; Hachtel, J.A.; et al. Theoretical and Experimental Insight into the Mechanism for Spontaneous Vertical Growth of ReS$_2$ Nanosheets. *Adv. Funct. Mater.* **2018**, *28*, 1801286. [CrossRef]

79. Zhang, H.; Wang, S.; Yu, J. Low-Symmetry Two-Dimensional ReS$_2$ and its Heterostructures: Chemical Vapor Deposition Synthesis and Properties. *Prog. Chem.* **2022**, *34*, 1440–1452.

80. Gao, J.; Li, L.; Tan, J.; Sun, H.; Li, B.; Idrobo, J.C.; Singh, C.V.; Lu, T.M.; Koratkar, N. Vertically Oriented Arrays of ReS$_2$ Nanosheets for Electrochemical Energy Storage and Electrocatalysis. *Nano Lett.* **2016**, *16*, 3780–3787. [CrossRef]

81. Kang, Y.B.; Han, X.; Kim, S.; Yuan, H.; Ling, N.; Ham, H.C.; Dai, L.; Park, H.S. Structural Engineering of Ultrathin ReS$_2$ on Hierarchically Architectured Graphene for Enhanced Oxygen Reduction. *ACS Nano* **2021**, *15*, 5560–5566. [CrossRef]

82. He, X.; Liu, F.; Hu, P.; Fu, W.; Wang, X.; Zeng, Q.; Zhao, W.; Liu, Z. Chemical Vapor Deposition of High-Quality and Atomically Layered ReS$_2$. *Small* **2015**, *11*, 5423–5429. [CrossRef] [PubMed]

83. Liu, L.; Chu, H.; Zhang, X.; Pan, H.; Zhao, S.; Li, D. Heterostructure ReS$_2$/GaAs Saturable Absorber Passively Q-Switched Nd:YVO$_4$ Laser. *Nanoscale Res. Lett.* **2019**, *14*, 112. [CrossRef] [PubMed]

84. Butanovs, E.; Kuzmin, A.; Piskunov, S.; Smits, K.; Kalinko, A.; Polyakov, B. Synthesis and characterization of GaN/ReS$_2$, ZnS/ReS$_2$ and ZnO/ReS$_2$ core/shell nanowire heterostructures. *Appl. Surf. Sci.* **2021**, *536*, 147841. [CrossRef]

85. Zhang, Y.; Liu, Y.; Cheng, P.; Song, W.; Zhang, X.; Rong, S.; Gao, X.; Zhou, G.; Zhang, Z.; Liu, J. Universal substrate growth of Ag-modified ReS$_2$ as visible-light-driven photocatalyst for highly efficient water disinfection. *Chem. Eng. J.* **2022**, *430*, 132918. [CrossRef]

86. Zhou, G.; Wu, Q.; Wu, L.; Liu, L.; Wang, D.; Wang, P. Reaction kinetic acceleration induced by atomic-hybridized channels in carbon quantum dot/ReS$_2$ composites for efficient Cr(VI) reduction. *Appl. Catal. B* **2022**, *300*, 119807. [CrossRef]

87. Zhao, Y.; Song, W.; Li, Z.; Zhang, Z.; Zhou, G. A new strategy: Fermi level control to realize 3D pyramidal NiCo-LDH/ReS$_2$/n-PSi as a high-performance photoanode for the oxygen evolution reaction. *J. Mater. Chem. C* **2022**, *10*, 3848–3855. [CrossRef]

88. Ha, E.; Liu, W.; Wang, L.; Man, H.W.; Hu, L.; Tsang, S.C.; Chan, C.T.; Kwok, W.M.; Lee, L.Y.; Wong, K.Y. Cu$_2$ZnSnS$_4$/MoS$_2$-Reduced Graphene Oxide Heterostructure: Nanoscale Interfacial Contact and Enhanced Photocatalytic Hydrogen Generation. *Sci. Rep.* **2017**, *7*, 39411. [CrossRef]

89. Li, L.; Salvador, P.A.; Rohrer, G.S. Photocatalysts with internal electric fields. *Nanoscale* **2014**, *6*, 24–42. [CrossRef]

90. Wu, Y.; Wang, H.; Sun, Y.; Xiao, T.; Tu, W.; Yuan, X.; Zeng, G.; Li, S.; Chew, J.W. Photogenerated charge transfer via interfacial internal electric field for significantly improved photocatalysis in direct Z-scheme oxygen-doped carbon nitrogen/CoAl-layered double hydroxide heterojunction. *Appl. Catal. B* **2018**, *227*, 530–540. [CrossRef]

91. Bellus, M.Z.; Li, M.; Lane, S.D.; Ceballos, F.; Cui, Q.; Zeng, X.C.; Zhao, H. Type-I van der Waals heterostructure formed by MoS$_2$ and ReS$_2$ monolayers. *Nanoscale Horiz.* **2017**, *2*, 31–36. [CrossRef]

92. Wang, F.; Hu, J.; Liang, R.; Lei, W.; Lou, Z.; Pan, X.; Lu, B.; Ye, Z. Novel ReS$_2$/g-C$_3$N$_4$ heterojunction photocatalyst formed by electrostatic self-assembly with increased H$_2$ production. *Int. J. Hydrogen Energy* **2022**, *47*, 29284–29294. [CrossRef]

93. Hu, J.; Li, X.; Qu, J.; Yang, X.; Cai, Y.; Yang, T.; Yang, F.; Li, C.M. Bifunctional honeycomb hierarchical structured 3D/3D ReS$_2$/ZnIn$_2$S$_4$-Sv heterojunction for efficient photocatalytic H$_2$-evolution integrated with biomass oxidation. *Chem. Eng. J.* **2023**, *453*, 139957. [CrossRef]

94. Reza Gholipour, M.; Dinh, C.T.; Beland, F.; Do, T.O. Nanocomposite heterojunctions as sunlight-driven photocatalysts for hydrogen production from water splitting. *Nanoscale* **2015**, *7*, 8187–8208. [CrossRef] [PubMed]

95. Saeed, M.; Uddin, W.; Saleemi, A.S.; Hafeez, M.; Kamil, M.; Mir, I.A.; Sunila; Ullah, R.; Rehman, S.U.; Ling, Z. Optoelectronic properties of MoS$_2$-ReS$_2$ and ReS$_2$-MoS$_2$ heterostructures. *Phys. B* **2020**, *577*, 411809. [CrossRef]

96. Zhang, Y.; Yan, Y.; Shen, G.; Hong, K. Synthesis of type-II heterojunction films between ReS$_2$ and XS$_2$ (X = Mo, W) with high electrocatalystic activities in dye-sensitized solar cells. *Catal. Commun.* **2022**, *170*, 106497. [CrossRef]

97. Zhang, W.; Mohamed, A.R.; Ong, W.-J. Z-Scheme Photocatalytic Systems for Carbon Dioxide Reduction: Where Are We Now? *Angew. Chem. Int. Ed.* **2020**, *59*, 22894–22915. [CrossRef]

98. Abdul Nasir, J.; Munir, A.; Ahmad, N.; ul Haq, T.; Khan, Z.; Rehman, Z. Photocatalytic Z-Scheme Overall Water Splitting: Recent Advances in Theory and Experiments. *Adv. Mater.* **2021**, *33*, 2105195. [CrossRef]

99. Wang, L.; Bie, C.; Yu, J. Challenges of Z-scheme photocatalytic mechanisms. *Trends Chem.* **2022**, *4*, 973–983. [CrossRef]

100. Di, T.; Xu, Q.; Ho, W.; Tang, H.; Xiang, Q.; Yu, J. Review on Metal Sulphide-based Z-scheme Photocatalysts. *ChemCatChem* **2019**, *11*, 1394–1411. [CrossRef]

101. Zhang, G.; Wang, Z.; Wu, J. Construction of a Z-scheme heterojunction for high-efficiency visible-light-driven photocatalytic CO$_2$ reduction. *Nanoscale* **2021**, *13*, 4359–4389. [CrossRef]

102. Liu, H.; Xu, B.; Liu, J.M.; Yin, J.; Miao, F.; Duan, C.G.; Wan, X.G. Highly efficient and ultrastable visible-light photocatalytic water splitting over ReS$_2$. *Phys. Chem. Chem. Phys.* **2016**, *18*, 14222–14227. [CrossRef] [PubMed]

103. Wang, Y.; Shi, R.; Song, K.; Liu, C.; He, F. Constructing a 2D/2D interfacial contact in ReS$_2$/TiO$_2$ via Ti–S bond for efficient charge transfer in photocatalytic hydrogen production. *J. Mater. Chem. A* **2021**, *9*, 23687–23696. [CrossRef]

104. Lin, B.; Ma, B.; Chen, J.; Zhou, Y.; Zhou, J.; Yan, X.; Xue, C.; Luo, X.; Liu, Q.; Wang, J.; et al. Sea-urchin-like ReS$_2$ nanosheets with charge edge-collection effect as a novel cocatalyst for high-efficiency photocatalytic H$_2$ evolution. *Chin. Chem. Lett.* **2022**, *33*, 943–947. [CrossRef]

105. Guo, L.; Yu, G.; Zhao, H.; Xing, C.; Hu, Y.; Chen, T.; Li, X. Construction of heterojunctions between ReS$_2$ and twin crystal Zn$_x$Cd$_{1-x}$S for boosting solar hydrogen evolution. *New J. Chem.* **2021**, *45*, 5137–5145. [CrossRef]

106. Shi, S.; Sun, Z.; Hu, Y.H. Synthesis, stabilization and applications of 2-dimensional 1T metallic MoS$_2$. *J. Mater. Chem. A* **2018**, *6*, 23932–23977. [CrossRef]

107. Kwak, I.H.; Kwon, I.S.; Debela, T.T.; Seo, J.; Ahn, J.-P.; Yoo, S.J.; Kim, J.-G.; Park, J.; Kang, H.S. Two-dimensional MoS$_2$–melamine hybrid nanostructures for enhanced catalytic hydrogen evolution reaction. *J. Mater. Chem. A* **2019**, *7*, 22571–22578. [CrossRef]

108. Liu, L.; Wu, J.; Wu, L.; Ye, M.; Liu, X.; Wang, Q.; Hou, S.; Lu, P.; Sun, L.; Zheng, J.; et al. Phase-selective synthesis of 1T' MoS$_2$ monolayers and heterophase bilayers. *Nat. Mater.* **2018**, *17*, 1108–1114. [CrossRef]

109. Yu, Y.; Nam, G.H.; He, Q.; Wu, X.J.; Zhang, K.; Yang, Z.; Chen, J.; Ma, Q.; Zhao, M.; Liu, Z.; et al. High phase-purity 1T'-MoS$_2$- and 1T'-MoSe$_2$-layered crystals. *Nat. Chem.* **2018**, *10*, 638–643. [CrossRef]

110. Ran, J.; Chen, L.; Wang, D.; Talebian-Kiakalaieh, A.; Jiao, Y.; Adel Hamza, M.; Qu, Y.; Jing, L.; Davey, K.; Qiao, S.-Z. Atomic-Level Regulated Two-Dimensional ReSe$_2$: A Universal Platform Boosting Photocatalysis. *Adv. Mater.* **2023**, e2210164. [CrossRef]

111. Huang, Q.; Yang, J.; Qi, F.; Zhang, W.; Zhang, N.; Liang, Z.; Liu, J.; Tian, C.; Tang, X.; Wu, D.; et al. Visible light driven photocatalytic reduction of CO$_2$ on Au-Pt/Cu$_2$O/ReS$_2$ with high efficiency and controllable selectivity. *Chem. Eng. J.* **2022**, *437*, 135299. [CrossRef]

112. Li, X.; Wang, X.; Hong, J.; Liu, D.; Feng, Q.; Lei, Z.; Liu, K.; Ding, F.; Xu, H. Nanoassembly Growth Model for Subdomain and Grain Boundary Formation in 1T′ Layered ReS$_2$. *Adv. Funct. Mater.* **2019**, *29*, 1906385. [CrossRef]

113. Ho, C.H.; Huang, Y.S.; Tiong, K.K. In-plane anisotropy of the optical and electrical properties of ReS2 and ReSe2 layered crystals. *J. Alloys Compd.* **2001**, *317–318*, 222–226. [CrossRef]

114. Parasuraman, P.S.; Ho, J.-H.; Lin, M.-H.; Ho, C.-H. In-Plane Axially Enhanced Photocatalysis by Re$_4$ Diamond Chains in Layered ReS$_2$. *J. Phys. Chem. C* **2018**, *122*, 18776–18784. [CrossRef]

115. Liu, W.; Wang, P.; Ao, Y.; Chen, J.; Gao, X.; Jia, B.; Ma, T. Directing Charge Transfer in a Chemical-Bonded BaTiO$_3$ @ReS$_2$ Schottky Heterojunction for Piezoelectric Enhanced Photocatalysis. *Adv. Mater.* **2022**, *34*, e2202508. [CrossRef]

116. Li, H.; Liang, Z.; Deng, Q.; Hu, M.T.; Du, N.; Hou, W. Facile Construction of Defect-rich Rhenium Disulfide/Graphite Carbon Nitride Heterojunction via Electrostatic Assembly for Fast Charge Separation and Photoactivity Enhancement. *ChemCatChem* **2019**, *11*, 1633–1642. [CrossRef]

117. Tu, S.; Guo, Y.; Zhang, Y.; Hu, C.; Zhang, T.; Ma, T.; Huang, H. Piezocatalysis and Piezo-Photocatalysis: Catalysts Classification and Modification Strategy, Reaction Mechanism, and Practical Application. *Adv. Funct. Mater.* **2020**, *30*, 2005158. [CrossRef]

118. Nosaka, Y.; Nosaka, A.Y. Generation and Detection of Reactive Oxygen Species in Photocatalysis. *Chem. Rev.* **2017**, *117*, 11302–11336. [CrossRef]

119. Wang, W.; Huang, G.; Yu, J.C.; Wong, P.K. Advances in photocatalytic disinfection of bacteria: Development of photocatalysts and mechanisms. *J. Environ. Sci.* **2015**, *34*, 232–247. [CrossRef]